Perovskite Solar Cells Go Bifacial - Mutual Benefits for Efficiency and Durability

Zhaoning Song, Chongwen Li, Lei Chen, and Yanfa Yan**

Zhaoning Song, Chongwen Li, Lei Chen, Yanfa Yan
University of Toledo, Wright Center for Photovoltaics Innovation and Commercialization, Department of Physics and Astronomy
2801 W Bancroft St, Toledo OH 43606, USA
E-mail: zhaoning.song@utoledo.edu; yanfa.yan@utoledo.edu

Keywords: perovskites, bifacial solar cells, albedo, building-integrated photovoltaics, bifacial tandem solar cells

Abstract

Bifacial solar cells hold the potential to achieve a higher power output per unit area than conventional monofacial devices without significantly increasing manufacturing costs. However, efficient bifacial designs are challenging to implement in inorganic thin-film solar cells because of their short carrier lifetimes and high rear surface recombination. The emergence of perovskite photovoltaic (PV) technology creates a golden opportunity to realize efficient bifacial thin-film solar cells, owing to their outstanding optoelectronic properties and unique features of device physics. More importantly, transparent conducting oxide electrodes can prevent electrode corrosion by halide ions, mitigating one major instability issue of the perovskite devices. In this perspective, we summarize the theory of bifacial PV devices and review the advantages of bifacial perovskite solar cells, such as high power output, enhanced device durability, and low economic and environmental costs. We also discuss the limitations and challenges for bifacial perovskite solar cells. Finally, we advocate the awareness of bifacial solar cells as a feasible commercialization pathway of perovskite PV for mainstream solar power generation and building-integrated PV and suggest future research directions.

1. Introduction

The past decade has witnessed rapid development in photovoltaic (PV) technologies and the widespread deployment of PV systems. The global installation of PV modules reached 139 gigawatts (GW) in 2020, bringing the accumulated global PV capacity to more than 760 GW.[1] Solar energy has been playing an increasingly important role in the world's energy portfolio. With strong forward momentum, it is becoming a key contributor in the global transition to decarbonized electricity generation. Given the speed of progress in lowering manufacturing costs and increasing the performance and reliability of different PV technologies, the growth toward multi-terawatt (TW) scale PV is expected in the coming years.[2, 3] To achieve sustainable PV manufacturing and deployment at the multi-TW scale, all of the established and future commercial PV technologies need to advance further in terms of a substantial increase in PV module power generation, reduction in module prices, and improvement in long-term reliability, eventually realizing low levelized costs of electricity (LCOE) that are compatible with standard electricity prices in the energy market. The PV industry's future development necessitates increased attention to emerging techniques with the potential to achieve high power generation at low costs.

Increasing the power output per unit area of solar panels at low additional manufacturing costs is crucial for further lowering the PV-generated electricity price. One of the simplest and inexpensive strategies for increasing the power output density of a solar panel is to harvest reflected and diffuse sunlight from the ground by employing bifacial designs. The concept of bifacial solar cells can date back to the 1960s, but the momentum to bring bifacial solar panels to the market has been gradually realized in the last decade as one of the latest technological advances in PV manufacturing.[4] The mainstream crystalline silicon (c-Si) PV module manufacturers are now producing bifacial silicon solar modules based on different cell

technologies. The trend shows that bifacial solar cells and modules are increasingly important in today's PV market and may soon become the cost-effective PV standard.[5]

Unlike c-Si solar cells, efficient bifacial designs have not been demonstrated in commercial inorganic thin-film PV technologies because the polycrystalline inorganic thin films suffer from short carrier lifetimes and high rear surface recombination, limiting their bifacial PV performance. Metal halide perovskite solar cells (PSCs) have generated great interest in the PV research and industry, owing to their fast-growing power conversion efficiencies (PCEs),[6] outstanding optoelectronic properties,[7] ease of production,[8] low estimated manufacturing costs,[9] and readiness to take steps toward commercialization.[10] Within a decade, PSCs have rapidly evolved from a newcomer to a leading competitor to rival other established PV technologies.

The development of PSCs opens up a golden opportunity to realize efficient bifacial thin-film solar cells. **Figure 1** depicts the bifacial architecture for PSCs, summarizes the unique optoelectronic properties of perovskites that enable high bifacial performance, and highlights the advantages of bifacial PSCs. Employing the bifacial device architecture can boost the power generation of PSCs by collecting more sunlight. More importantly, the transparent conducting oxide (TCO) electrodes used in the bifacial architectures possess high halide corrosion resistance and diffusion blocking effects, mitigating one major instability issue of PSCs and, therefore, enabling long-term stability. The enhanced device performance and durability are critical to delivering low LCOE and environmental impacts. Additionally, bifacial perovskite PV devices have broad applications in different fields, including bifacial solar modules for utility-scale, commercial, and residential solar projects and building-integrated photovoltaics (BIPV). If it succeeds, bifacial perovskite PV will become a disruptive player in the PV market in the future. Although considerable efforts are directed toward developing semitransparent bifacial PSCs and perovskite tandem solar cells, there is no systematic understanding of bifacial

PSCs' operation principles, production, and commercial applications. A comprehensive guideline to rationally design bifacial PSCs, accurately assess their bifacial performance, and identify and overcome the hurdles to their commercialization is in urgent demand.

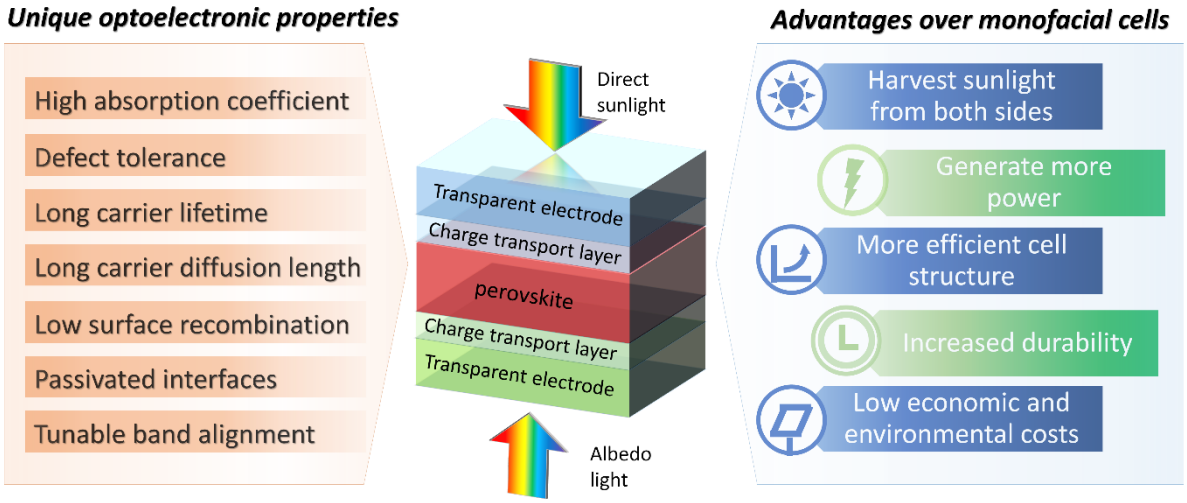

Figure 1. Schematic structure of a bifacial perovskite solar cell, the unique properties of metal halide perovskites, and the advantages of bifacial perovskite solar cells.

In this perspective, we hope to convey a complete picture of the advantages and challenges of the bifacial perovskite PV technology. We first discuss the working principle, key concepts, accurate assessment, and theoretical and practical efficiency limits of bifacial solar cells. We then summarize the unique optoelectronic properties of metal halide perovskites that enable their excellent bifacial PV performance and briefly review the surge of bifacial perovskite PV applications. Lastly, we outline the current limitations and shortcomings of bifacial perovskite PV and provide our views on the future research and development directions that can realize the full potential of bifacial PSCs.

2. Working Principles of Bifacial Solar Cells

Bifacial solar cells can collect light incidents on both the front and rear surfaces, enabling higher output power density than their monofacial counterparts. Thermodynamically, a bifacial solar cell in operation is just a concentrated solar cell at a low injection (light intensity < 2 suns) because collecting the additional photons from the rear surface increases the number of photons absorbed in the cell. In practice, bifacial illumination provides a different charge generation profile in the absorber layer than concentrated single-side illumination, and consequently, has unique recombination and charge transport properties that govern PV performance. This section briefly discusses the key concepts of bifacial solar cells, standardize measurement methods, theoretical and achievable equivalent efficiency gains, and some device examples based on conventional PV materials.

2.1. Characterization of Key Parameters

Bifacial solar cells are fabricated with two transparent electrodes or have two light-permeable surfaces, allowing light incidents on both the front and rear sides of the devices (Figure 1). Consequently, the PCE of a bifacial solar cell can be characterized independently under one sun illumination on the front (**Figure 2a**) or rear (Figure 2b) side. One of the key parameters to characterize bifacial solar cells is the bifaciality factor (φ), which is defined as the PCE ratios:

$$\varphi = \eta_{rear}/\eta_{front} \quad (1)$$

where η_{rear} and η_{front} are efficiencies of a bifacial solar cell under the rear and front side illumination, respectively. Typically, the front is the primary side to collect direct sunlight, and the front-conversion efficiency is equal to or higher than the rear-conversion efficiency. Therefore, φ typically has a range of 0 to 1. A higher φ value indicates a better albedo light conversion capability for a given solar cell.

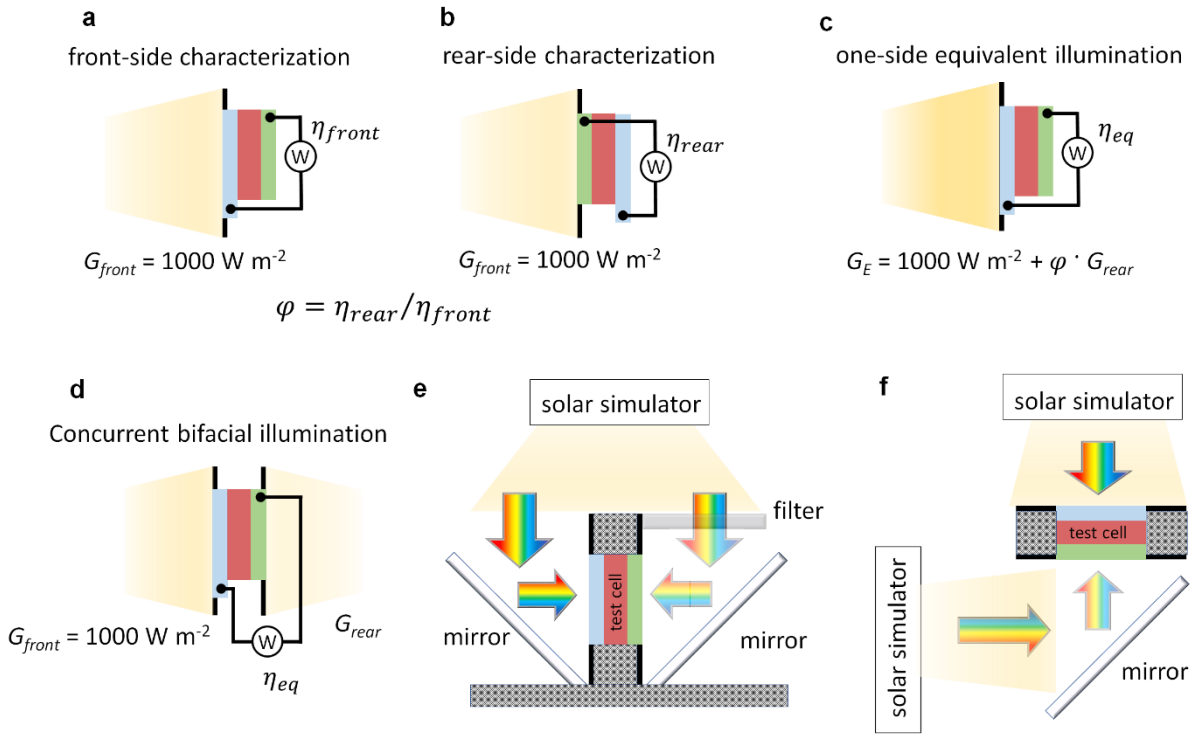

Figure 2. Schematic illustration of bifacial solar cell efficiency characterization. (a) Front-side, (b) rear-side, and (c) one-side equivalent efficiency measurements using a single illumination source. Bifaciality factor (φ) is defined as the ratio of the rear to front efficiencies. (d) bifacial equivalent efficiency measured under concurrent bifacial illumination. (e, f) schematic measurement system setups for standard bifacial solar cell characterization under simultaneous bifacial illumination using (e) one or (f) two solar simulators.

Unlike regular monofacial solar cells, there is no consensus on the standardized measurement protocols of bifacial solar cells in research laboratories. Most researchers only report bifaciality determined by the ratio of the rear to front side efficiencies measured separately but not measure the devices under simultaneous bifacial illumination. To better characterize bifacial solar cells under bifacial illumination on both front and rear sides, parameters have been proposed to clarify the rear side illumination condition.[11] The irradiance gain (g) and irradiance factor (χ), which are used to describe the additional back irradiation, are defined as:

$$g = (G_{rear} + G_{front})/G_{front} \quad (2)$$

$$\chi = G_{rear}/G_{front} = g - 1 \quad (3)$$

where G_{front} and G_{rear} are front and back illumination light intensities for the specific bifacial application. Normally, the AM1.5G illumination with one sun intensity, corresponding to a power density of 1000 W m^{-2}, is used for G_{front}, whereas G_{rear} can be variable depends on different application scenarios. In practical applications, G_{rear} is mainly from the surface reflection of direct sunlight. Therefore, χ is also referred to as the albedo factor.

Bifacial solar cells under both-side illumination can be characterized using the bifacial equivalent efficiency, which is defined as the equivalent efficiency of a monofacial cell that can generate the same power density as the bifacial cell under the same testing condition. Bifacial equivalent efficiency (η_{eq}) can be estimated after independent front and rear PCE measurements using this equation:

$$\eta_{eq} = \eta_{front} + \eta_{rear} \cdot \chi \quad (4)$$

The equivalent efficiency provides an assessment of the end-use benefits of bifacial solar cells, i.e., to estimate energy yield under certain installation conditions, and, thus, is more frequently used than the absolute PCE considering the total input photon energy. Besides, the bifacial efficiency gain (*BEG*) is defined as the relative increase in equivalent PCE under bifacial illumination compared with monofacial illumination:

$$BEG\ (\%) = (\eta_{rear} \cdot \chi)/\eta_{front} = \varphi \cdot \chi \cdot 100 \quad (5)$$

A critical issue with bifacial PV is the uncertain standard and characterization protocols, especially in academic research laboratories. The International Electrotechnical Commission (IEC) technical specification 60904-1-2: "Measurement of current-voltage characteristics of bifacial photovoltaic (PV) devices" proposes two methods for the current-voltage (I-V) characterization.[4] The first is an equivalent single-side illumination measurement using a typical solar simulator as in monofacial solar cell characterization (Figure 2c).[11] In this

approach, an equivalent irradiance is used to compensate irradiance gain from the rear-side illumination, as defined by:[12]

$$G_{eq} = G_{front} + (\frac{I_{sc,rear}}{I_{sc,front}}) \cdot G_{rear} \approx 1000\ W\ m^{-2} + \varphi \cdot G_{rear} \quad (6)$$

where $I_{SC,\ rear}$ and $I_{SC,\ front}$ are short-circuit currents of a bifacial solar cell under rear and front side illumination, respectively. The front-side illumination is fixed at one sun intensity (1000 W m^{-2}), and the equivalent rear-side light intensity is 0.1 or 0.2 sun, corresponding to a light intensity of 100 or 200 W m^{-2}. Because this method does not require extra accessories other than standard monofacial cell characterization tools, it is used for characterizing commercial bifacial PV modules. However, the actual operation of bifacial solar cells is not necessarily a simple linear summation of separately measured front and rear side efficiency in proportion to their irradiance conditions. The second method measures a test cell under concurrent bifacial illumination consisting of the front irradiance at one sun intensity and the rear at 0.1 or 0.2 sun intensity (Figure 2d). A typical bifacial measurement system can be set up with one solar simulator with a filter and mirrors to split the simulated solar radiation (Figure 2e)[4, 13] or two solar simulators simultaneously illuminated from both sides of the test device (Figure 2f).[4, 14]

2.2. Theoretical and Practical Efficiency Gains

2.2.1. Equivalent Circuit and Theoretical Efficiency Limits

The equivalent circuit for a bifacial solar cell is the same as a single-diode solar cell model with an additional current source to represent the photocurrent generated from the rear-side illumination (**Figure 3a**). In brief, the J-V curve of a bifacial solar cell can be described by:

$$J = J_0\ \left[\exp\left(\frac{V+JR_S}{nkT}\right) - 1\right] + \left(\frac{V+JR_S}{R_{sh}}\right) - J_{ph,front} - J_{ph,rear} \quad (7)$$

where J_0 is dark saturation current density, R_s and R_{sh} are series and shunt resistances, respectively, n is the ideality factor of a diode, k is the Boltzmann constant, T is the temperature of the cell, and $J_{ph,\ front}$ and $J_{ph,\ rear}$ are the photocurrent densities under the front and rear side illumination, respectively. The sum of the last two terms gives the total photocurrent density (J_{ph}).

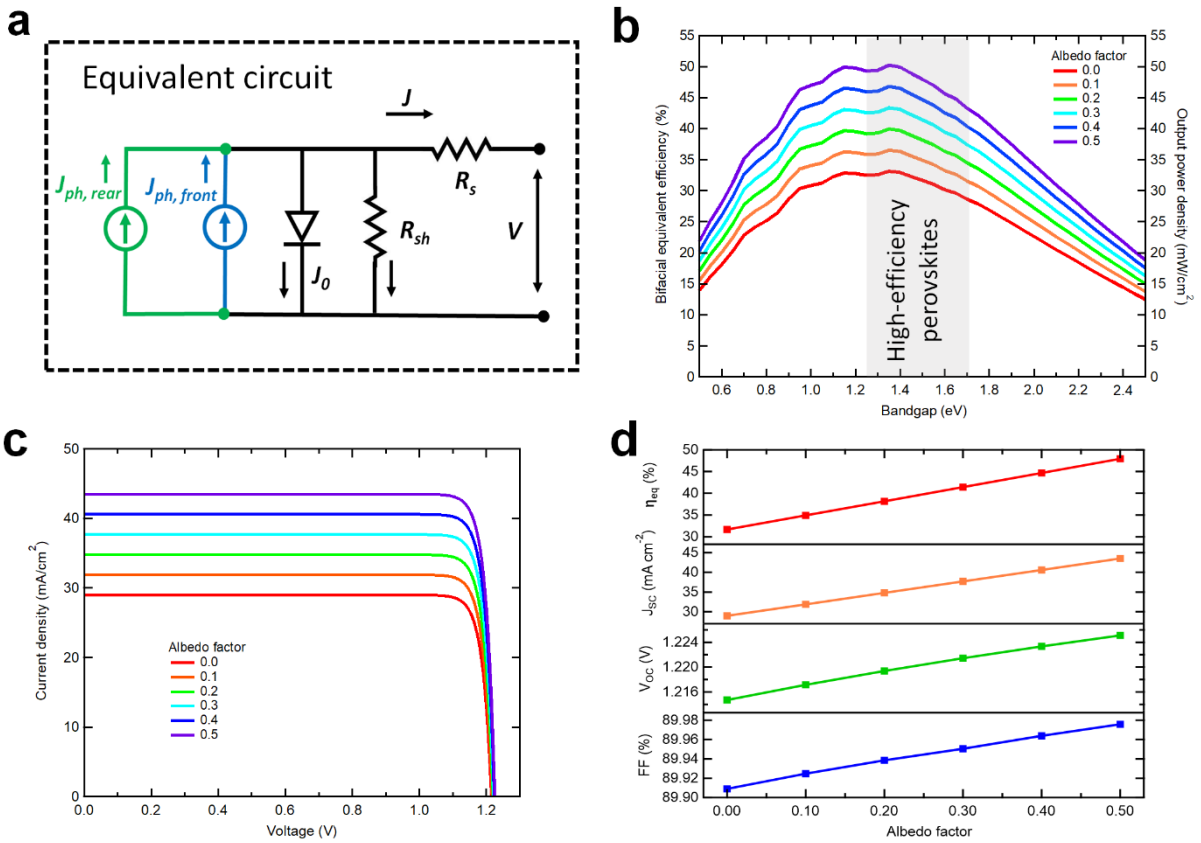

Figure 3. Theoretical model and efficiency limits of a bifacial solar cell under different bifacial illumination conditions. (a) Equivalent circuit of a bifacial solar cell. (b) Detailed balance efficiency limits of bifacial solar cells as a function of absorber bandgap and albedo conditions. Reproduced with permission.[15] Copyright 2021, Royal Society of Chemistry. (c) J-V curves and (d) PV parameters (η_{eq}, J_{SC}, V_{OC}, and FF) of an ideal solar cell with a bandgap of 1.5 eV under different bifacial illumination conditions.

The detailed balance efficiency limit for bifacial solar cells can be calculated by solving the diode equation. In brief, for an ideal solar cell, the impact of n, R_s, and R_{sh} is omitted. J_0 is determined only by the total rate of recombination owing to the blackbody radiation from both sides of the cell with energy above its bandgap:[15]

$$J_0 = 2q \int_{E_g}^{\infty} \frac{1}{\exp(h\nu/kT)-1} \frac{2\pi\nu^2}{c^2} d\nu \quad (8)$$

where q is the unit charge, E_g is the bandgap of the absorber layer, h is the Planck constant, υ is the frequency of a photon, and c is the speed of light.

The total light photocurrent density under bifacial illumination is determined by:

$$J_{ph} = \int_{\lambda_i}^{1240/E_g} \left[G_{front}(\lambda) + G_{rear}(\lambda) \times \varphi\right] d\lambda \quad (9)$$

where λ_i and λ are the shortest wavelength for the illumination spectrum and the wavelength of a photon, respectively.

Figure 3b plots the theoretical efficiency limits of ideal bifacial solar cells with different absorber E_g values and different bifacial illumination conditions (χ = 0.0 to 0.5).[15] The shaded region highlights the bandgap range (1.25 to 1.70 eV) for high-efficiency (> 20%) PSCs. Bifacial solar cells in this bandgap range show significant efficiency gains with an additional rear-side irradiance. For example, Figure 3c displays the J-V curves of an ideal solar cell with an E_g of 1.5 eV, close to the bandgap of ubiquitous formamidinium lead iodide ($FAPbI_3$)-based perovskites, under different rear-side irradiance conditions. Figure 3d summarizes the variations in the PV parameters as a function of the albedo factor. For an ideal solar cell, increasing the rear-irradiance intensity not only proportionally increases short-circuit current density (J_{SC}) but also slightly increases open-circuit voltage (V_{OC}) and fill factor (FF), leading to a higher PCE. The trend is the same as in the relationship between light intensity and PCE for concentrated solar cells.[16]

2.2.2. Factors limiting bifacial efficiency

For a practical bifacial solar cell, J_{ph} is greatly influenced by the spectral response of the device under two-side illumination. Equation 9 can be modified to

$$J_{ph} = \int_{\lambda_i}^{1240/E_g} \left[G_{front}(\lambda) \times EQE_{front}(\lambda) + G_{rear}(\lambda) \times EQE_{rear}(\lambda)\right] d\lambda \qquad (10)$$

where EQE_{front} and EQE_{rear} are the external quantum efficiencies (EQE) under front-side and rear-side irradiance, respectively. Different PV technologies exhibit various bifacial responses to the solar spectrum. All major c-Si PV technologies, including passivated emitter rear contact (PERC), silicon heterojunction with an intrinsic thin layer (HIT), interdigitated back contact (IBC), and tunnel oxide passivated contacts (TOPCon), have already realized bifacial applications with high PCEs exceeding 20% and high φ values in the range of 0.75 to 0.95.[4, 17] For instance, a typical bifacial c-Si HIT cell shows a high φ of 0.93 with similar EQE curves under the front and rear illumination (**Figure 4a**).[18] The high bifaciality of the c-Si HIT cell is enabled by the long carrier lifetime (100 μs to ms) and diffusion length (up to 300 μm) in the bulk Si and the heterojunction passivation by intrinsic thin layers, which ensure that the photogenerated carriers can be collected by selective contacts before recombining.[19]

In contrast to c-Si cells, conventional thin-film solar cells, such as CdTe and CIGS, typically exhibit poor bifaciality. For instance, Figure 4b compares EQE curves of a bifacial CdS/CdTe solar cell under front-side and rear-side illumination.[20] The front-side EQE shows a relatively high response across the wavelength range of CdTe absorption, while the rear-side EQE only exhibits a weak response with gradually increasing efficiencies at longer wavelengths, corresponding to the lower energy photons that are absorbed closer to the p-n heterojunction. The poor bifaciality is mainly attributed to the relatively short carrier lifetimes, unfavorable band bending at the rear interface, and high rear surface recombination velocity of polycrystalline CdTe, as illustrated in Figure 4c.[19] Because of the low bifaciality, thin-film PV technologies based on CdTe,[20-23] CIGS,[24-26] organic PV,[27, 28] and dye-sensitized solar cells[29, 30] have only been considered for flexible, low-weight, semitransparent applications,[17] but have not yet commercialized for high-efficiency bifacial PV modules.

Unlike the other thin-film PV technologies, metal halide perovskite thin films possess long minority carrier lifetimes and diffusion lengths, low rear surface recombination velocities, and proper band alignment and passivation at the interfaces. Consequently, typical bifacial PSCs exhibit comparable EQE curves under the front and rear illumination, as shown in Figure 4d, and high bifaciality.[15] The unique properties of perovskite that enable such high bifaciality are discussed in Section 3.

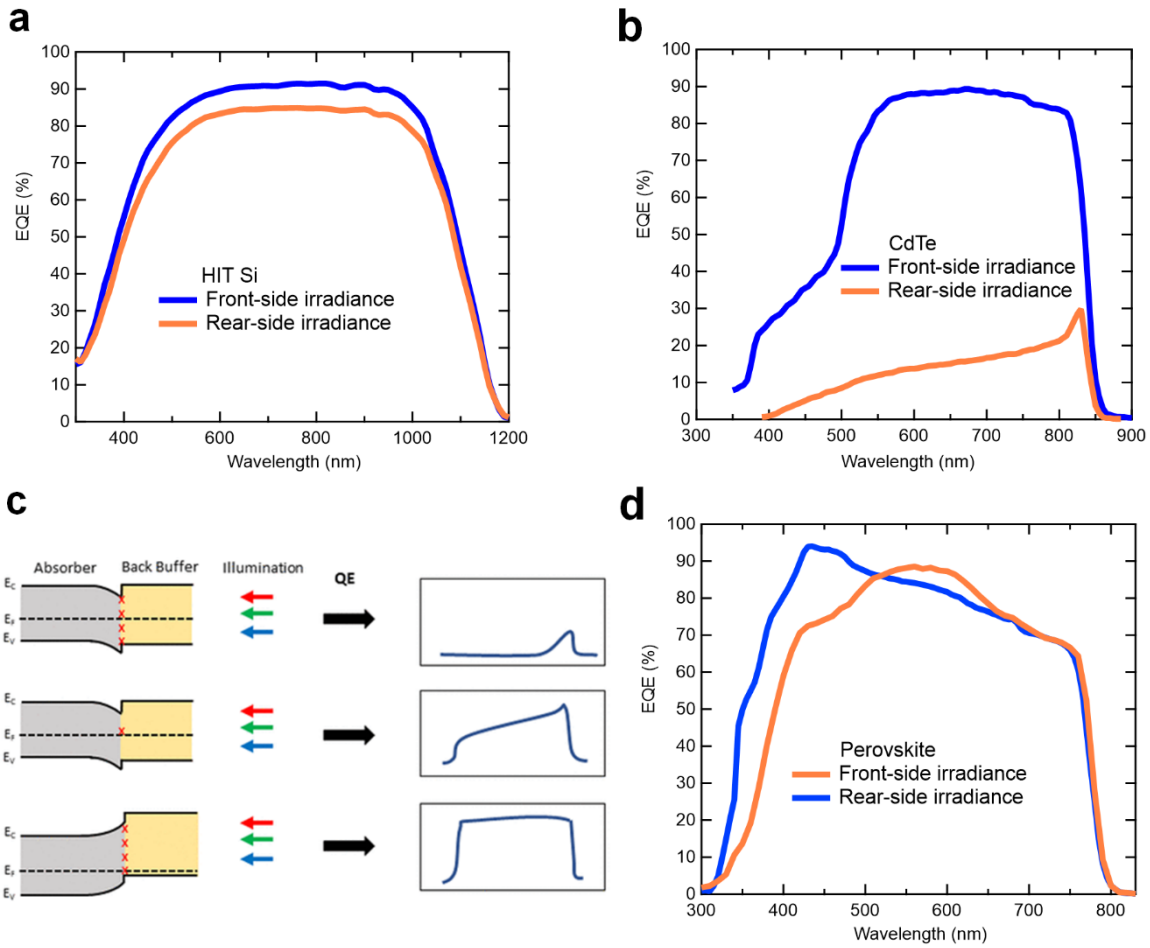

Figure 4. Spectral responses of bifacial solar cells. (a) EQE curves of a bifacial HIT Si cell under the front and rear side illumination. Data was adapted from a conference presentation.[18] (b) EQE curves of a bifacial CdTe solar cell under the front and rear side illumination. Data was adapted from our previous work.[20] (c) Schematic illustration of factors limiting the rear-side EQE of a thin-film solar cell. Reproduced with permission.[19] Copyright 2020, American Chemical Society. (d) EQE curves of a bifacial perovskite solar cell under the front and rear side illumination. Data was adapted from our previous work.[15]

2.2.3. Albedo Conditions and Efficiency Gains

The power gain from a bifacial solar cell compared with a monofacial equivalent depends on the amount of light incident on the rear surface and the rear-side efficiency. In practical applications, the fraction of sunlight reflected by the ground or a reflective back surface provides the rear-side irradiance of a bifacial solar cell. Albedo measures how well a surface reflects light and is generally defined as the ratio between the power of the reflected light and the power of the total incoming light. When the albedo is high, the number of photons from the rear side illumination becomes significant to the total power output of a bifacial solar cell. **Figure 5a** shows the reflection spectra of common ground materials under normal incidence,

adapted from the record in NASA's ECOSTRESS Spectral Library.[31] Figure 5b compares their average albedo values in the typical perovskite absorption range (300 to 850 nm). Common ground materials (e.g., grass, sand, foam, and concrete) show an average albedo of 0.1 to 0.3, which is why IEC sets the irradiance factor to 0.1 or 0.2 for the standardized indoor characterization of bifacial solar cells. However, it is still recommended for outdoor applications to use reflectance spectra measured at the installation site to estimate the real bifacial gains. A combined theoretical and experimental analysis shows that the power output of bifacial solar cells under spectral albedo is different from wavelength-independent albedo.[32]

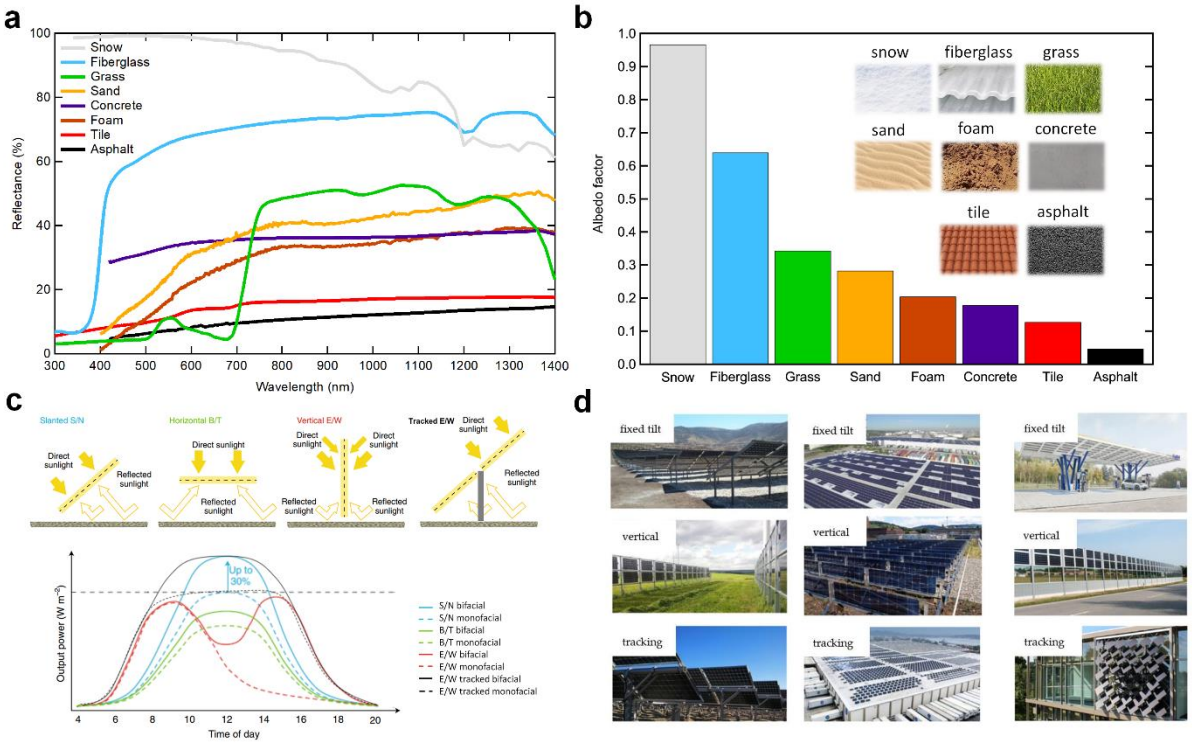

Figure 5. Albedo conditions and practical installations of bifacial PV modules. (a) Reflectance spectra and (b) albedo factor of common ground materials. The reflectance data is adapted from NASA's ECOSTRESS Spectral Library. [31] (c) Possible installation of bifacial modules and comparison of power gains. (d) Photos of bifacial PV module installations. Panels (c) and (d) are reproduced with permission.[5] Copyright 2021, MDPI.

Ground albedo is the most significant uncertainty for bifacial efficiency gain. Albedo light depends strongly on the surface of the ground, the geographic location of the installation, and the tilt angle of the module. The angle of incident light varies with the time of the day, and the solar spectrum changes with the time of the year, both contributing to the constantly altering rear-side irradiance. Bifacial PV modules have various implementation approaches, resulting

in different bifacial gains. Figure 5c summarizes the common bifacial PV module configurations, including fixed-tilt, horizontal, vertical, and tracked, and compares typical daily power generation gains of bifacial over monofacial modules for each configuration.[5] The energy yield of a bifacial PV module can be up to 30% higher than monofacial ones under optimal conditions.[33] A power output gain of up to 50% for bifacial PV modules has been demonstrated with a highly reflective ground material and specially designed installation arrangement.[34] Figure 5d shows the photos of representative examples for bifacial PV installations at utility, commercial, and residential scales implemented in different ways.[5] With increasing installation capacity, bifacial PV modules are becoming a popular choice in the market.[5]

3. Advantages of Bifacial Perovskite PVs

Unlike conventional thin-film PV materials, metal halide perovskites possess a unique set of characteristics that make them so fascinating in bifacial PV applications. The outstanding optoelectronic properties, including strong optical absorption, defect tolerance, long charge carrier lifetimes and diffusion lengths, low surface recombination velocities, easily passivated interfaces, and proper band alignment at the interfaces, enable efficient charge carrier generation and collection in perovskite absorber layers under the front and rear side illumination. The diversity in device architectures combined with a variety of materials synthesis methods allows the fabrication of bifacial PSCs in different film stack sequences. Additionally, the chemical robustness and compactness of transparent conducting oxide (TCO) electrodes provide additional benefits of protecting rear electrode from halide-induced correction and blocking the ingress of water and the egress of volatile perovskite decomposition byproducts, enabling a long device lifetime for bifacial PSCs. Lastly, strong material sustainability and low-cost fabrication techniques offer low-cost advantages in economic and environmental aspects.

3.1. Unique Features of Metal Halide Perovskites

3.1.1. Excellent optoelectronic properties

Metal halide perovskites exhibit direct bandgap transitions with strong optical absorption coefficients.[35] The absorption coefficient is the most crucial parameter dictating the light absorption in a PV material. The high absorption in lead halide perovskites is enabled by a combination of the allowed transition matrix elements and a high joint density of states (DOS).[36] **Figure 6a** compares the schematic band structures of Si, GaAs, and lead halide perovskite.[37] The indirect bandgap Si has a low α value because of the forbidden transition at the band edges. GaAs and perovskite both have allowed direct transitions. However, in the conduction band, lead halide perovskites show less dispersive Pb (6*p*) orbitals than the s-bands of Ga and As in GaAs and a higher DOS, which enable a strong direct bandgap *p*-*p* transition.[38] Consequently, Pb halide perovskites show stronger optical absorption than Si and GaAs (Figure 6b). The high absorption of halide perovskites allows PSCs to harvest most of the capturable sunlight in an absorber layer with a thickness less than 1 μm and minimize the travel distance of photogenerated carriers before they are collected, which is critical for governing the charge generation and transport properties in bifacial solar cells.

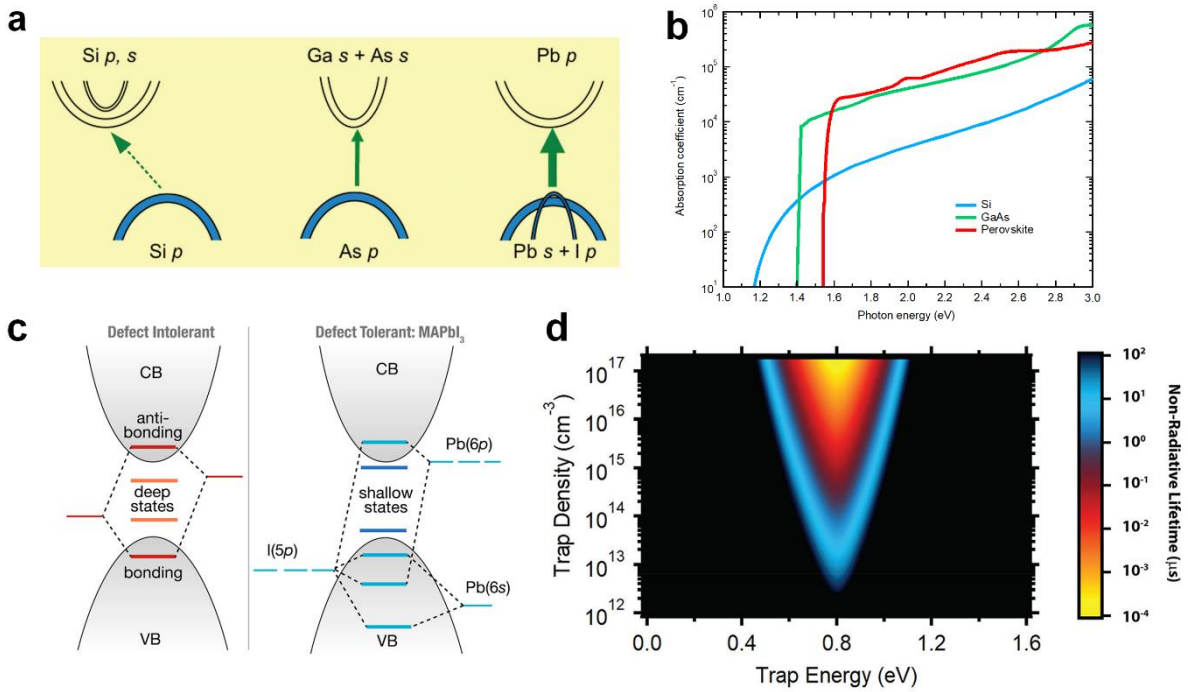

Figure 6. Optoelectronic properties of perovskite compared with conventional inorganic PV materials. (a) Schematic band structure of Si, GaAs, and Pb perovskites. Reproduced with permission.[37] Copyright 2015, American Chemical Society. (b) Absorption coefficient comparison of Si, GaAs, and perovskite. (c) Comparison of the electronic band structures and defects of conventional inorganic semiconductors and metal halide perovskites. Reproduced with permission.[39] Copyright 2017, American Chemical Society. (d) Calculated nonradiative lifetime as a function of trap density and trap energy level. Reproduced with permission.[40] Copyright 2019, American Chemical Society.

Metal halide perovskites show high defect tolerance for defect-assisted nonradiative recombination losses. Defects with energy levels at the center of the bandgap of a semiconductor annihilate charge carriers through nonradiative recombination known as the Shockley-Read-Hall (SRH) recombination.[41, 42] Reducing defect density in the absorber layer of a solar cell is critical to reduce the nonradiative recombination rate and prolong the lifetime of photogenerated charge carriers so that they can be efficiently extracted. In conventional inorganic PV materials, such as group IV (e.g., Si), III-V (e.g., GaAs), and II-VI (CdTe), the bonding and antibonding states form valence band maximum (VBM) and conduction band minimum (CBM), respectively, whereas defect levels are relatively deep (Figure 6c, left).[39] Unlike conventional PV materials, lead halide perovskites exhibit unique defect tolerance behavior.[43] Due to high symmetry crystal structure and Pb's electronic configuration ($6s^2 6p^0$), the CBM is mainly derived from Pb (6*p*) and I (5*p*) states, while the VBM is mainly derived from the Pb (6*s*) and I (5*p*) antibonding states. As a result, defects with low formation energies only create shallow defect levels (Figure 6c, right).[38, 39] These sallow defects in metal halide perovskites are mostly benign and do not constitute nonradiative recombination centers that limit carrier lifetime even at a high density of $10^{15} – 10^{16}$ cm^{-3} (Figure 6d).[40, 44] Additionally, grain boundaries of Pb halide perovskites have electrically clean defect properties similar to point defects.[38] Consequently, polycrystalline Pb halide perovskite thin films typically exhibit long carrier lifetimes up to several to tens of μs,[45-47] which are much higher than the 1-100 ns

scale lifetimes for other conventional inorganic thin-film PV materials and are close to that of single crystals.[48]

Lead halide perovskites exhibit balanced ambipolar carrier transport properties. The strong hybridization of s-p antibonding coupling, strong spin-orbit coupling, and lone-pair s-orbitals lead to small effective masses for both electrons and holes.[38] For instance, theoretical calculations predict that $MAPbI_3$ possesses light electron (0.15 to 0.23 m_e) and hole (0.12 to 0.30 m_e) effective masses, where m_e is the free electron mass.[49-51] The light carrier masses for both electrons and holes provide the means for high-mobility carrier transport. Additionally, most Pb halide perovskites possess a low intrinsic carrier concentration on the order of 10^{10} to 10^{12} cm^{-3}.[52-54] The ionic nature of the perovskite crystal also provides a dielectric screening effect to suppress the Coulomb interactions between carriers and ionic defects in the lattice.[55] The low intrinsic scattering rates in the bulk perovskite, along with the extrinsic control of grain boundaries and imperfections via engineering the deposition processes, contribute to the decent charge carrier mobility values of a few to tens $cm^2\ V^{-1}\ s^{-1}$.[56] The combination of high mobility values, long carrier lifetimes, and small effective masses results in long carrier diffusion lengths of several μm,[57] which enable the thin-film device architectures for present high-efficiency PSCs.

3.1.2. Photocarrier Generation

The operation of a solar cell under illumination is governed explicitly by the generation, recombination, and transport of photoexcited carriers. One distinct difference between bifacial and monofacial solar cells is the photogenerated carrier profile in the absorber layer. The rear-side irradiance alters the carrier distribution profile in the absorber layer, which may yield a different conversion efficiency.

Figure 7a plots the wavelength-dependent photon absorption percentage rate in a representative mixed methylammonium (MA)/ formamidinium (FA) perovskite absorber layer[58] as a

function of the absorber thickness, using the absorption coefficient curve of the perovskite in Figure 6b.[59] The light blue color outline represents the required depth for less than 1% normalized photon density, corresponding to > 99% light absorption. Based on this light absorption distribution, we calculate the density of photons absorbed in the perovskite layer under AM1.5G solar illumination, as shown in Figure 7b. The spectral integration of the photon density profile results in a critical factor in solar cell device analysis, i.e., the depth-dependent photocarrier generation rate profile (Figure 7c). The photogeneration profile defines the non-equilibrium charge carrier distribution in a solar cell, which can be used as the initial values to solve the drift-diffusion equations and simulate the device's PV performance. The accumulated photon density (or maximum short-circuit photocurrent density) is calculated by the integrating of generation profile with depth (Figure 7d). The analysis shows that a typical perovskite layer with a thickness of ~300 nm is sufficient to absorb 80% of usable photons. Increasing the absorber thickness to ~800 nm can increase the harvest ratio to ~95%. This thickness range is in good agreement with the historical evolution of state-of-the-art PSCs reported in the literature.[60]

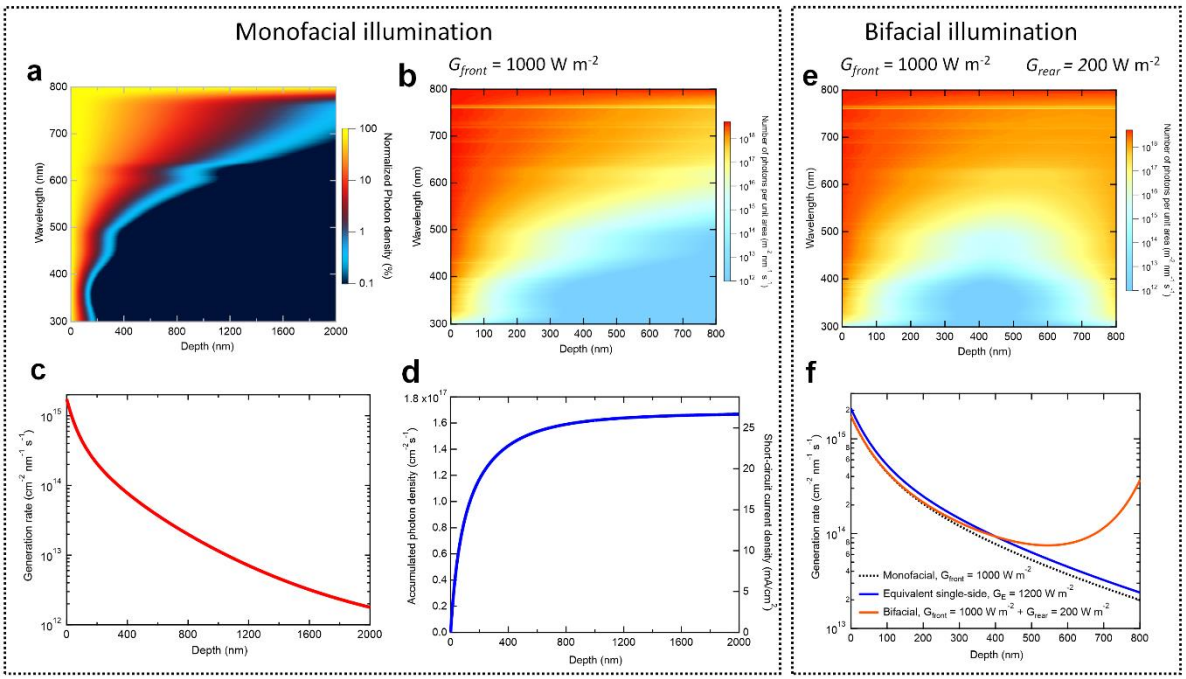

Figure 7. Light absorption and charge carrier generation in a perovskite absorber layer under monofacial and bifacial illumination. (a) Normalized photon density and (b) photon generation rate as a function of wavelength and perovskite absorber depth in a monofacial PSC under AM1.5 solar irradiance. (c) Photogeneration rate under AM1.5 solar irradiance and (d) accumulated photon density and integrated short circuit current density in a perovskite absorber as a function of the perovskite absorber depth. (e) Photon generation rate as a function of wavelength and perovskite absorber depth in a bifacial PSC under bifacial illumination with an albedo factor of 0.2. (f) Comparison of photogeneration rate of a bifacial PSC under monofacial, equivalent single-side, and bifacial illumination conditions.

Under bifacial illumination conditions, the photocarrier generation profile in a perovskite absorber layer is quite different from the monofacial situation. Figure 7e shows the wavelength-dependent photon generation rate as a function of absorber depth in an 800 nm perovskite layer under a concurrent bifacial illumination with G_{front} = 1000 W m^{-2} and G_{rear} = 200 W m^{-2}. The photocarrier density generated at the rear surface (depth = 800 nm) significantly increases, especially at short wavelengths. The photogeneration rate as a function of depth (Figure 7f) shows that the increase in photocarrier density due to bifacial illumination is mainly within ~ 300 nm from the rear surface (Figure 7f, orange curve), which differs significantly from the charge carrier profile under the equivalent single-side illumination with the same irradiance intensity (Figure 7f, blue curve). Therefore, to achieve high PCE under bifacial illumination, it

is critical to tune the band alignment and interface recombination at the rear surface of the perovskite layer to collect these extra photogenerated carriers close to the back surface.

3.1.3. Photocarrier Recombination and Collection

The quasi-Fermi energy splitting in a semiconductor is determined by the excess charge carrier densities under illumination, which in turn, depends on the effective carrier lifetime (τ_{eff}). **Figure 8a** shows a schematic of charge carrier recombination and extraction processes in a perovskite solar cell, consisting of an anode, a hole transport layer (HTL), a perovskite absorber layer, an electron transport layer (ETL), and a cathode.[61] The effective carrier lifetime in a perovskite layer can be determined as:[62, 63]

$$\frac{1}{\tau_{eff}} = \frac{1}{\tau_{bulk}} + \frac{1}{\tau_{surf}} \quad (10)$$

where τ_{bulk} are τ_{surf} bulk and surface lifetimes, respectively. The bulk lifetime can be expressed as:

$$\frac{1}{\tau_{bulk}} = \frac{1}{\tau_{SRH}} + \frac{1}{\tau_{rad}} + \frac{1}{\tau_{Auger}} \quad (11)$$

where τ_{SRH}, τ_{rad}, and τ_{Auger}, and are trap-assisted SRH, radiative, and Auger recombination lifetimes, respectively. The former two recombination types are also referred to as monomolecular and bimolecular recombination because trap-induced recombination involves a charge carrier, either an electron or a hole, and an electrically active trap, while radiative recombination needs both.

Figure 8b depicts the estimated contributions to τ_{bulk} with different carrier injection intensities.[63] Under a common bifacial irradiance condition (Figure 7f), the excess carrier concentrations at the front and rear surfaces are ~10^{16} and ~10^{15} cm^{-3}, respectively. The bulk lifetime in the range of a few hundred ns to 1 μs is limited mainly by the SRH recombination. Figure 8c shows the calculated carrier diffusion lengths as a function of carrier density and monomolecular (trap-assisted) recombination rate.[64] The arrows in the figure indicate the

achievable diffusion lengths under AM1.5 irradiance for each τ_{SRH} condition. Based on the calculation, diffusion lengths of more than 1 μm are expected for most PSCs, which are sufficient to cover the whole thickness of the perovskite absorber layer, allowing charge carriers generated throughout the perovskite absorber layer to be efficiently collected.

In general, the bulk lifetime and diffusion length are dominated by trap-assisted recombination in a perovskite layer, which is determined by the spatial and energetic distribution of the defects within the bandgap of perovskite.[65] Recent studies demonstrated that some detrimental defects in perovskites could be reduced or eliminated via engineering perovskite deposition processes and passivation by introducing additives.[66, 67] A sufficiently long lifetime of up to 18 μs has been demonstrated in polycrystalline perovskite thin films.[45-47]

Because of the relatively long bulk lifetime and a short thickness of a perovskite film, the recombination of photoexcited carriers will eventually occur at the surfaces of the perovskite layer. Therefore, the surface recombination velocity (SRV) of a perovskite layer plays an essential role in determining τ_{eff} and PCE of the corresponding bifacial device. Figure 8d plots surface lifetime as a function of layer thickness and surface recombination velocity.[62] For typical polycrystalline perovskite films with a lifetime of several hundreds of ns, low SRVs of 10 to 100 cm s^{-1} are expected,[62] which are similar to that of passivated Si wafers.[68]

A low SRV, particularly at the rear surface of an absorber layer, is the key to enable the high bifaciality of thin-film solar cells.[19] Figure 8e shows the impact of rear-side SRV on the performance of bifacial PSCs under the front and rear illumination simulated by a one-dimensional solar cell simulation program (SCAPS-1D)[69] using parameters reported elsewhere.[65] The results show that the PV performance of the device decreases with increasing rear-side SRV. When the rear-side SRV is high, the detrimental impact is more severe under the rear-side illumination than front-side illumination owing to more pronounced drops in J_{SC} and *FF*. Consequently, a higher rear-side SRV leads to a lower bifaciality factor. When the

SRV is lower than 100 cm s^{-1}, the difference in the PCE of the device under the front and rear-side illumination is small, and thus a high bifaciality can be obtained. Figure 8f further compares the detailed generation and recombination current densities of bifacial PSCs with rear-side SRVs of 10 and 10^4 cm s^{-1} under rear-side illumination and various voltages. At a high SRV (10^4 cm s^{-1}), the interface recombination dominates the total recombination current, and it increases with voltage. The high interface recombination current significantly limits the *FF* and V_{OC} of the device. In contrast, the device with a low SRV (10 cm s^{-1}) is limited by the SHR recombination in the bulk film. The long carrier lifetime and low SRV guarantee high bifaciality for PSCs, enabling higher power generation gains under bifacial irradiance.

Thanks to high absorption coefficients, long carrier lifetimes and diffusion lengths, and low surface recombination velocities, many bifacial perovskite solar cells achieved high bifaciality factors close to 0.95 and even approaching 1.[15, 70-73] These high bifaciality factors are competitive or even superior to that of state-of-the-art c-Si bifacial solar cells.[4] The capability to achieve such a high bifaciality is the foundation of the success of bifacial PSCs.

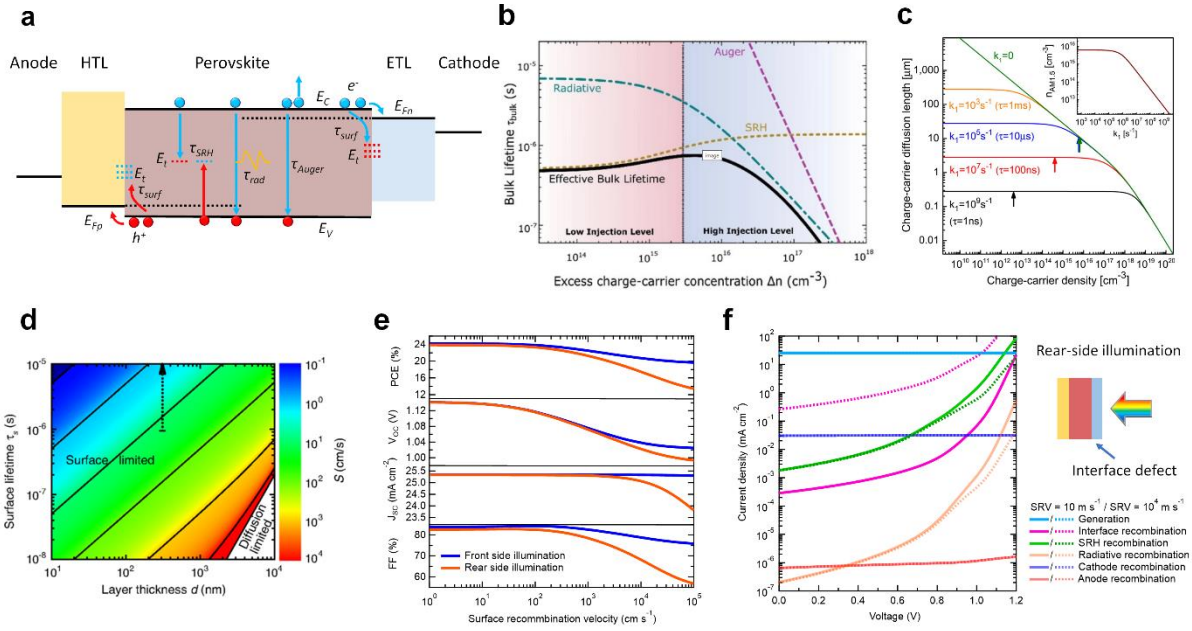

Figure 8. Charge carrier recombination in PSCs. (a) Schematic of charge carrier recombination and collection processes in a PSC. (b) Effective bulk lifetime as a function of excess charge carrier concentration. Reproduced with permission.[63] Copyright 2019, Wiley. (c) Calculated

charge-carrier diffusion lengths as a function of monomolecular recombination rate and charge carrier density. Reproduced with permission.[64] Copyright 2015, American Chemical Society. (d) Surface lifetime as a function of layer thickness and surface recombination velocity. Reproduced with permission.[62] Copyright 2016 American Physical Society. (e) Simulated PV parameters of a bifacial perovskite solar cell with different surface recombination velocities (SRVs) at the perovskite/ETL interface (rear-surface) under the front and rear side illumination. (f) Calculated generation and recombination current of the bifacial perovskite solar cell with an SRV of 10 and 10^4 cm s^{-1}.

3.1.4 Diversity in Device Architectures

The established thin-film PV technologies based on CdTe and CIGS have little flexibility in their device architectures, fabrication sequences, and materials selections.[74] High-efficiency CdTe and CIGS cells have to be produced in the superstrate (i.e., light incident from the glass substrate) and substrate (i.e., light incident from the top TCO) configurations, respectively.[75] The cells fabricated in the opposite sequence typically result in considerably inferior performance.[76, 77] Bifacial applications have been explored in these inorganic PV technologies, but the PCE and bifaciality factors are relatively low, mainly due to short carrier lifetimes and high recombination at the back interfaces.[19]

Unlike the inorganic thin-film PV technologies, one unique feature of PSCs is that they possess flexibility in diverse device structures, a wide selection of component layer materials, and various device fabrication techniques. The technical advances in monofacial PSCs with the p-i-n and n-i-p configurations have already paved the way to introduce light into the perovskite layer from both n-type electron transport layer (ETL) and p-type hole transport layer (HTL).[78] The successful intersurface passivation strategies applied to both top and bottom surfaces of perovskite layers minimize the surface recombination velocity of perovskites.[67] Therefore, bifacial configurations can be easily implemented in PSCs with both n-i-p (**Figure 9a** and 9b)[79, 80] and p-i-n (Figure 9c and 9d) [70, 81] configurations with wide selections of the HTLs (e.g., Spiro-TTB, spiro-OMeTAD, MoO_3, NiO_x, PTAA), ETLs (e.g., SnO_2, C_{60}, ZnO, PCBM), and transparent electrode materials (e.g., ITO, In_2O_3:H, ZnO:Al).

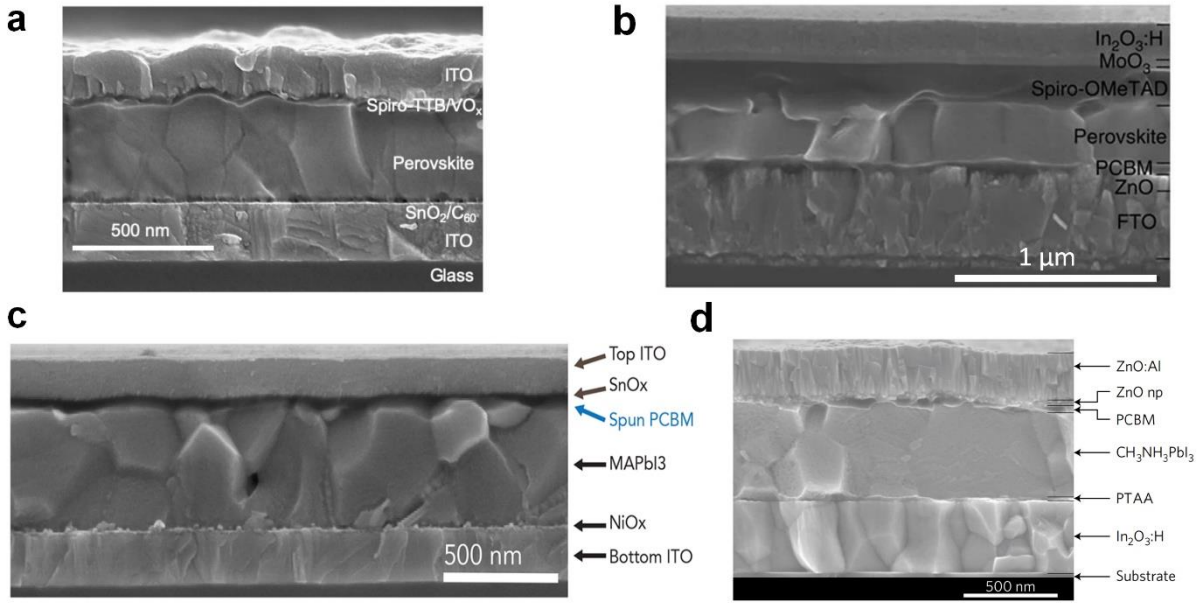

Figure 9. Bifacial PSC device structures. (a, b) Cross-sectional SEM images of bifacial PSCs in n-i-p configurations. Panel (a) is reproduced with permission.[79] Copyright 2019, Royal Society of Chemistry. Panel (b) is reproduced with permission.[80] Copyright 2015, Springer Nature. (c, d) Cross-sectional SEM images of bifacial PSCs in p-i-n configurations. Panel (c) is reproduced with permission.[81] Copyright 2018, American Chemical Society. Panel (d) is reproduced with permission.[70] Copyright 2016, Springer Nature.

3.2. Benefits for Long-Term Stability

Apart from a higher power output per unit area, bifacial PSCs possess inherent device stability advantages compared with monofacial devices using an opaque metal back contact. The perovskites are notoriously susceptible to degradation induced by moisture-induced phase degradation,[82-84] decomposition triggered by the loss of volatile species,[85, 86] and corrosion of metal electrodes due to the reaction with halides.[87-89] The use of robust and compact TCO rear electrodes provides a holistic solution to all these degradation routes.[90, 91]

The rear electrode comprising a compact and conformal metal oxide layer forms a permeation barrier to prevent external moisture from penetrating the cell interior and the egress of volatile constituents of halide perovskites, enabling thermally and environmentally stable bifacial PSCs (**Figure 10a**).[84, 92] The inclusion of a self-encapsulating oxide layer (e.g., SnO_x) can significantly improve the stability of PSCs against moisture even in the liquid form (Figure

10b).[93] The employment of an ITO electrode also improves thermal stability in the ambient atmosphere. Figure 10c shows that the active area covered by the ITO layer remained dark, while the uncovered areas around already thermally decomposed into yellow PbI_2 after operation at 150 ˚C under illumination for 90 s.[90]

The presence of the ITO layer effectively retarded the perovskite decomposition and the release of volatile decomposition species. The confinement of volatile substitutes may promote the "self-healing" of perovskites and prolong the lifetime.[94, 95] Recent studies demonstrated that PCSs with a combination of an ITO rear electrode, a low elastic modulus encapsulant, and a glass-glass sealing can withstand thermal cycling and damp heat tests.[96, 97] For instance, Figure 10d shows the PCE evolutions and photos of encapsulated PSCs with ITO back electrodes for accelerated lifetime tests for 1000 hours under the dry heat (85 ˚C and 25% RH) and damp heat (85 ˚C and 85% RH) conditions.[97] The insignificantly changes in PCE and the appearance of the cells show that the ITO electrode with proper encapsulating packaging is capable of protecting PSCs from heat and moisture-induced degradation. Moreover, sputtered TCO electrode has also been employed to improved thermal and environmental stability in air-sensitive mixed tin-lead iodide perovskite solar cells without compromising device efficiency.[98]

Ion migration in PSCs can induce the corrosion and degradation of metallic electrodes and eventually lead to the failure of the devices.[99] The electrochemical reactions between halide species and metallic electrodes can lead to the formation of insulating decomposition byproducts at the interface and the addition of excess halide vacancies and extrinsic metal defects to the perovskite layer.[99] It is well known that commonly used noble and transition metal electrodes (e.g., Ag,[100-102], Au,[103] Cu,[104, 105] Al,[88, 89] etc.) react with halide perovskites and introduce metallic impurities,[87] which is a significant source of intrinsic device degradation under operation. The long-term operation of PSCs requires a chemically stable

electrode, such as TCO layers. Because of the chemical inertness and robustness of these metal oxide layers, the TCO-based rear electrodes are free of corrosion by moisture in the air and halide species in the perovskite absorber layer. Figure 10e shows that the bare ITO layer has robust stability at an elevated temperature of 85 ˚C, while the addition of metal grids on the top of the ITO layer still shows some degree of degradation after 1000 hours of thermal aging.[81]

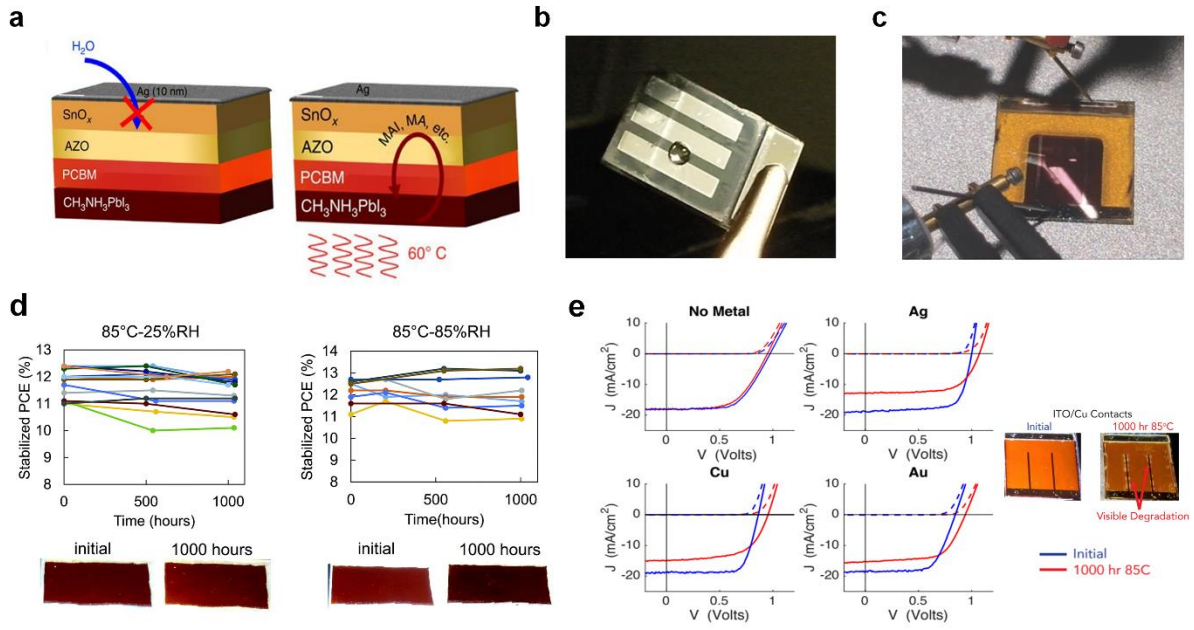

Figure 10. Stability improvement by using metal oxide top electrodes. (a) Schematic of a compact SnO_x layer prevents water ingress and volatile species egress. Reproduced with permission.[92] Copyright 2017, Springer Nature. (b) A photo of a drop of water on metal an oxide protected PSC. Reproduced with permission.[93] Copyright 2016, American Chemical Society. (c) A photo of a bifacial $MAPbI_3$ PSC working at 150 ˚C. Reproduced with permission.[90] Copyright 2016, WILEY. (d) Evolution of PCE and photos of bifacial PSCs aged under dry-heat and damp-heat conditions. Each curve represents an individual testing cell. Reproduced with permission.[97] Copyright 2018 Royal Society of Chemistry. (e) J-V curves of bifacial PSCs without and with metal grids (Ag, Cu, and Au) before and after 1000 hours of aging at 85 ˚C. The photos show the change of the ITO/Cu sample before and after the test. Reproduced with permission.[81] Copyright 2018, American Chemical Society.

3.3. Low Economic and Environmental Costs

The potential long-term stability and high power density will enable low economic and environmental costs of solar energy generation in the life cycle of bifacial PSCs. Perovskite PV modules are projected to be a low-cost PV leader because they can be manufactured with low-

cost materials and deposition techniques and have the potential to deliver lower LCOE compared with other electricity generation sources.[9, 106] With additional benefits in higher power generation and longer lifetime than monofacial PSCs and minimum additional costs associated with a transparent back contact,[15] bifacial perovskite PVs are expected to achieve even lower LCOEs in the long term. The energy payback time (EPBT) and global warming potential (GWP) metrics per energy generated from bifacial perovskite PV cells are also lower than other conventional PV technologies because of their higher energy yield and lower embedded energy, making them an environmentally friendly future PV technology.[107]

3.4. Versatile Bifacial perovskite PV Applications

3.4.1. Bifacial perovskite PV modules

High-efficiency bifacial PV modules are the primary potential application of bifacial PSCs. Benefiting from the high power generation and low manufacturing costs, bifacial perovskite PV modules are expected to be a low-cost leader in the PV panel market if their on-field durability can be demonstrated. The bifacial perovskite PV modules are likely to be built with thick formamidinium lead triiodide-based perovskite absorber layers with low transmittance of visible light (**Figure 11a**). This bifacial module design aims at maximizing the productivity of harvesting direct, reflected, and diffuse sunlight. The implementation of the bifacial perovskite PV modules for utility, commercial, and residential power generation is the same as what has been used for the current bifacial c-Si modules (Figure 11b). Their real-world performance will depend on the deployment scenarios with different amounts of albedo irradiance.[108, 109]

3.4.2. Semitransparent Bifacial PSCs

Bifacial PSCs can be made into semitransparent solar cells that absorb some photons and allow certain light transmittance. The transparency can be achieved by either making a thin perovskite absorber layer or tailoring its bandgap to allow more photons to pass through (Figure 11c).[110, 111] The colorful appearance of semitransparent bifacial PSCs can be tailored by controlling the

film stack thickness to achieve constructive optical interference at a given wavelength range (Figure 11d),[72, 112] which provides better aesthetics of bifacial PSCs for different BIPV applications, such as solar windows in buildings (Figure 11e).[113] For the applications of semitransparent bifacial PSCs, PCE and average transparency (AVT) are two figures of merit,[110] while the bifaciality is not considered as a critical parameter since there is not much rear irradiance. Recent review papers on semitransparent PSCs already provide a good summary of their progress and practical applications.[78, 112, 114]

3.4.3. Bifacial Perovskite Tandem Solar Cells

The application of bifacial PSCs can go beyond single-junction cells and realize in tandem configurations.[115] The tunable bandgap and the success of semitransparent PSCs enable the integration of a perovskite top cell with lower bandgap bottom cells (e.g., Si, CIGS, and low-bandgap perovskite) into tandem solar cells,[116-119] which can potentially overcome the thermodynamic efficiency limits of single-junction devices. The tandem cells can also be made using the bifacial designs, provided that the bottom cells have high bifaciality.[115] Currently, c-Si meet the criteria of both high PCEs and bifaciality and is suitable for the bottom cell of the bifacial perovskite tandem devices.

Bifacial perovskite tandem solar cells can be fabricated in two different tandem device configurations, including mechanically stacked four-terminal (4-T) and monolithically integrated two-terminal (2-T) tandem cells (Figure 11f).[116] For the 4-T tandem devices, the rear irradiance absorbed by the c-Si bottom cells directly results in a linear increase in extra power generation because the two cells in tandem work separately.[120, 121] For 2-T tandem devices, the rear-irradiance boosts the photocurrent in the bottom cell and thus allows the relaxation of the current-match constrains in the tandem design to achieve a high PCE.[122] Bifacial perovskite/Si tandem solar cells allow the use of the perovskite top cell with a lower bandgap than that used in a monofacial tandem, enabling enhanced PCE and elongating stability

due to reduced halide phase segregation.[122] Because of the higher power generation enabled by the bifacial feature, the cost benefits of bifacial perovskite/c-Si tandem cells are expected to be larger than their monofacial equivalent.[107, 115] or the real-world application of bifacial perovskite/Si modules, the installation type and geological conditions of the installation site needs to take into consideration to maximize the solar power generation gains (Figure 11g).[123]

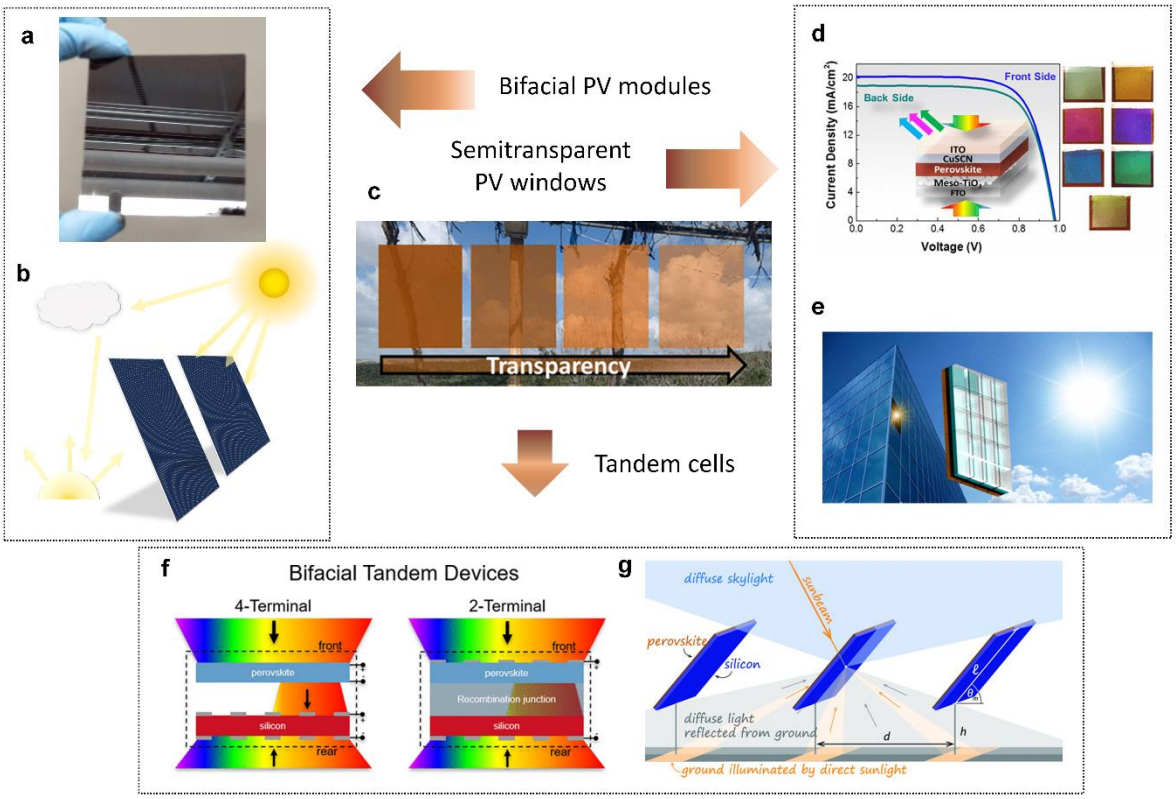

Figure 11. Bifacial perovskite PV applications. (a) Photo of a thick perovskite film with low transparency of visible light. (b) Schematic of bifacial perovskite PV module application. (c) Perovskite films with different transparency. Reproduced with permission.[110] Copyright 2020, American Chemical Society. (d) J-V curves and device structure of a semitransparent bifacial solar cell with photos showing tunable color by adjusting ITO thickness. Reproduced with permission.[72] Copyright 2019, American Chemical Society. (e) Image illustrating PV window application for semitransparent PSCs. Reproduced with permission.[113] Copyright 2017, American Chemical Society. (f) Schematic of 4-T and 2-T bifacial tandem cells comprising bifacial perovskite top cells. Reproduced with permission.[115] Copyright 2020, American Chemical Society. (g) Schematic of the installation of bifacial perovskite/Si tandem PV modules. Reproduced with permission.[123] Copyright 2021, Wiley.

4. Challenges of Bifacial Perovskite PV

Despite tremendous progress in the last decade, perovskite PV technology is still at the premature stage of development. There are several technological challenges to overcome before bifacial perovskite PV modules can gain an opportunity to enter the market. Major challenges and bottlenecks include (1) the optical and electrical losses, (2) TCO rear electrode processing damages, (3) bifacial module manufacturing and scalability, (4) device durability and reliability, and (5) toxicity and cost issues.

4.1. Optical and Electrical Losses

4.1.1. Optical losses

Optical and electrical losses are a major source of efficiency losses in bifacial PSCs because of more complex light paths and management in bifacial devices than monofacial cells (**Figure 12a**). The main optical losses include the reflection from both surfaces of a device, parasitic absorption in electrodes and charge transport layers, and incomplete light absorption in the perovskite absorber layer. Mitigating optical losses can significantly enhance the photocurrent, the most significant contributor to bifacial PV power gains. Therefore, light management strategies and proper design of materials and device structures are needed to overcome the challenges in improving light harvesting in the perovskite absorber layers.

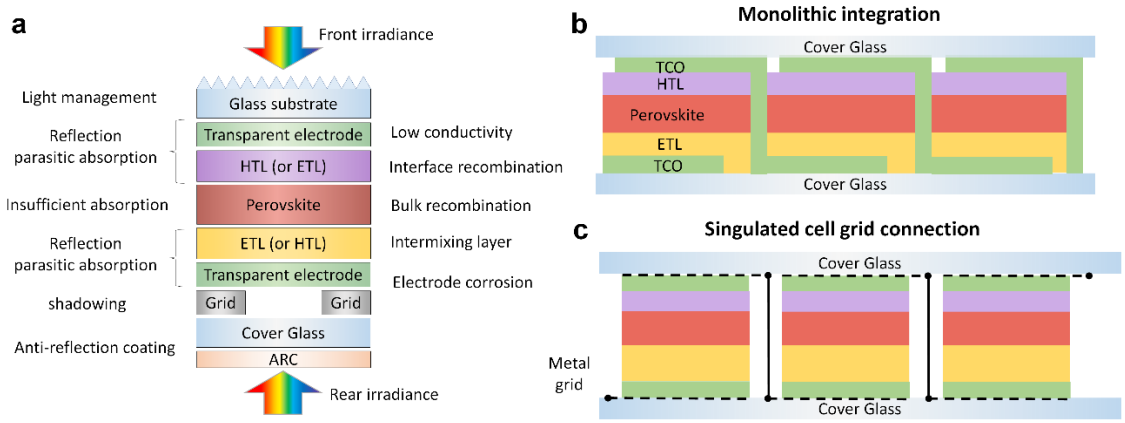

Figure 12. Bifacial perovskite module design. (a) Management of optical and electrical losses in a bifacial perovskite solar cell. Two possible bifacial perovskite module configurations: (b) monolithic integration and (c) singulated cell grid connection.

The total reflection of TCO coated glass substrates typically accounts for ~10% of optical losses due to the reflective index mismatch at the interfaces (refractive indices of 1, ~1.5, ~1.9 for air, glass, and ITO, respectively).[78] The reflection losses are doubled for bifacial PSCs under two-side irradiance, compromising their potential to deliver high output powers as promised. Optical modulation needs to be taken into consideration to maximize the light absorption in bifacial PSCs.[124] Common light management strategies to mitigate reflection losses include applying anti-reflection coatings (e.g., MgF_2)[73] and textured or nanostructured polymeric foils (e.g., polydimethylsiloxane (PDMS)).[125-127] The former changes the constructive and destructive optical interference to reduce light reflection at particular wavelengths, while the latter provides a broadband reflection reduction due to diffuse reflection and scattering at the light incident surface. Alternatively, a textured solar glass used in commercial c-Si modules can be considered for bifacial PSCs.[128] In addition to anti-reflection strategies, other optical manipulation strategies, including surface nanostructured enhanced light scattering,[129] surface plasmonic effects,[130] photonic nanostructures,[131] optical microcavity,[132] can be used to enhance light absorption in PSCs.

The parasitic absorption and series resistance losses in front and rear TCO layers are two primary sources for the power losses in bifacial PSCs. Typically, there is a tradeoff between the transmittance and electrical conductivity of transparent electrodes. Both the front and rear transparent electrodes need to achieve a certain thickness and doping levels to ensure sufficient electrical conductivity. As a result, parasitic absorption due to free carriers and impurities becomes significant. Moreover, because of the thermal instability of the perovskite layer, the annealing process for the TCO rear electrode that deposited on the perovskite absorber layer is generally omitted, leading to inferior optical transparency than high-temperature processed TCOs. To mitigate the parasitic light absorption issues, TCOs with relatively high electron mobility and a low carrier density, such as hydrogen-doped indium oxide (IO: H),[80, 133] indium

doped zinc oxide (IZO),[133, 134] and combined TCOs,[135] are employed as the rear electrode. Alternatively, some ultra-thin metal/dielectric film stacks,[136-138] metallic nanostructures (e.g., Ag nanowires),[139, 140] carbon nanostructures (e.g., graphene, nanotubes)[141-143] are also explored for the metal-oxide-free transparent electrodes. However, their optical and electrical properties are still inferior to the TCO electrodes.

The parasitic absorption and reflection losses in CTLs also contribute to the power losses in bifacial PSCs. Practical device architecture design needs to judiciously select materials based on their optical properties to minimize these optical losses in CTLs, which requires the accurate measurement of extinction coefficient (k) and refractive index (n) and the establishment of an optical database for all the component materials used in PSCs.[144, 145] Some CTLs that are commonly used in high-efficiency monofacial PSCs, such as spiro-OMeTAD and PCBM, have significant parasitic absorption of visible light and are not suitable for bifacial applications.[146, 147] Alternative materials, including spiro-TTB,[79] CuSCN,[72] PTAA/CuO_x,[148] and C_{60}/SnO_2,[15] can be utilized in bifacial PSCs to mitigate the parasitic absorption losses in the CTLs.

The optical losses can originate from the perovskite absorber layer due to insufficient absorption. The light absorption analysis (Figure 7) of perovskites shows that a minimum thickness of ~800 nm is needed to harvest ~95% of usable light. However, in high-efficiency monofacial PSCs, perovskite absorber thickness is mainly 500 to 700 nm. The high optical reflection of opaque metal electrodes (e.g., Au, Ag, and Cu) effectively increases the optical path of photons in the perovskite absorber layer and thus boosts light absorption. In contrast, the transparent electrodes of bifacial PSCs allow unabsorbed light to transmit through instead of bounce back. Therefore, to maximize the light absorption in perovskite and fulfill the potential of delivering high output power density, the bifacial solar cell requires a thicker absorber layer thickness than their monofacial counterparts. The technical advances in

preparing high-quality μm-thick perovskite layers will help meet this requirement for high-efficiency bifacial perovskite solar modules.[149, 150]

4.1.2. Electrical losses

The nonradiative recombination in the bulk of a perovskite absorber layer and interface recombination at the perovskite and CTLs interfaces are two major factors limiting the performance of PSCs.[151] The nonradiative recombination issues in the bulk perovskite have been significantly mitigated in the past few years through the technical progress in composition optimization, crystallinity improvement, grain size enhancement, and grain boundary passivation.[67] Questions remain on applying these engineering techniques to thicker perovskite layers produced by scalable deposition methods. Many interface passivation strategies have also been developed to reduce surface recombination velocity at the front and rear surfaces of a perovskite layer, showing substantial improvements in V_{OC} and *FF*. The interface passivation of both surfaces of a perovskite absorber layer is critical to enable high PCEs under illumination from both sides and a high bifaciality factor.

Another key factor contributing to the electrical losses in PSCs is the interfacial mixing layers, consisting of constitutes of perovskite and CTLs and voids.[144] The formation of a "dead" layer of the intermixing perovskite materials with a very high surface recombination velocity can lead to substantial losses in both J_{SC} and V_{OC}.[152, 153] To avoid the formation of this high recombination layer, the possible detrimental chemical reactions between CTLs and halide perovskites need to be prevented by incorporating interface passivation or isolation layer. Additionally, diffusion barrier layers are desired to stop the migration and mixing of halide anions with extrinsic impurities from CTLs and electrodes.[99]

One disadvantage of bifacial PSCs is the relatively high series resistance caused by the low conductivity of two TCO electrodes. This high series resistance leads to a higher electrical power loss with a higher photocurrent. Under bifacial illumination conditions, bifacial PSCs

suffer more from the series resistance loss than their monofacial counterparts with opaque metal electrodes. To overcome this issue, metal grids and fingers are employed onto the TCO electrodes to reduce the resistance for lateral photocurrent collection.[15] Reducing the single cell width of conventional monolithically integrated thin-film modules (Figure 12b) can effectively reduce the series resistance loss. Alternatively, the singulated substrate cell integration (Figure 12c) that used for flexible CIGS solar cells can be adapted for the production of bifacial PSCs.[154] Yet, the design of the metal grid and finger connections need to be optimized to balance the tradeoff between reduced series resistance and the optical loss due to their light shading effect. The metal grid and TCO design needs to be further explored for bifacial PSCs to minimize the loss caused by high series resistance.[155]

4.2. Challenges for Processing TCO Rear Electrodes

The energetic deposition of rear TCO electrodes by magnetron sputtering or e-beam evaporation presents a big challenge for producing efficient and stable bifacial PSCs. The harsh processing conditions, such as high temperature, plasma effect, ion bombardment, would greatly damage fragile perovskite and organic materials. Therefore, the deposition of TCO rear electrodes needs to be under control to minimize the chance of damaging the underneath layers.[73, 135] Previous studies suggest that appropriate buffer layers, such as evaporated MoO_x,[156-159] ZnO nanoparticles,[70, 90, 160] and ALD SnO_x,[81, 161] can provide robust protection for vulnerable perovskite materials and organic charge transport layers against processing damages. However, the additional buffer layer increases processing complexity and reduces production throughput. The introduction of the buffer layer also leads to higher parasitic absorption, resulting in a lower photocurrent under rear-side illumination. More recently, driven by remarkable progress of transparent PSCs and perovskite tandem solar cells, facile and damage-free sputtering methods have been developed, allowing direct deposition of appropriate TCO contacts on the functional layers of PSCs without damaging the cells.[73, 147, 162, 163] These

promising results of directly sputtered TCO rear electrodes open the possibility for producing efficient bifacial PSCs.

4.3. Modules Manufacturing and Scalability

Bifacial perovskite module design and manufacturing have specific challenges and barriers to overcome prior to the commercialization of this new technology. Currently, there is a substantial gap in PCE between small-area cells and large-area modules.[164] For bifacial perovskite PV modules, this gap is likely even wider because the conventional thin-film module design for monolithic integration of individual cell stripes is limited by the low conductivity of two TCO layers. The wafer-like cell integration approach used in flexible CIGS solar cells is a possible solution to overcome the issue of high TCO resistance. The design and optimization of busbars, metal fingers, and cell connections need to be taken into consideration. Additionally, to maximize the power generation in bifacial perovskite PV modules, the location for the junction box and the construction of shadowless mounting need to be accurately evaluated. Some of these challenges have been tackled by silicon PV companies, and their ideas and strategies can be learned by the perovskite stakeholders.

Another major challenge is the scalable manufacturing of large-area bifacial perovskite PV modules.[8] Scaling up the perovskite module production to industrially relevant levels and transferring the technology from the lab to the fab require certain criteria in the spatial uniformity, repeatability, and throughput deposition of each layer of materials in PSC film stacks. Efforts are being made to overcome the difficulty in preparing high-quality and homogeneous perovskite films using scalable deposition techniques in a scalable manufacturing environment. Recent advances in printing friendly techniques for fabricating PSCs, such as slot-die,[165-167] blading coating,[168] bar-coating,[169-171] and roll-to-roll printing,[172-174] have demonstrated high performance mini-modules, showing the promise of scalable manufacture of PSCs.

4.4. Device Reliability and Durability

The compact and dense TCO rear electrodes used in bifacial PSCs provide self-encapsulation to protect perovskite layers and significantly improve their device stability. Yet, to become commercially relevant, PSCs have to establish reliability and durability that can meet and compete with commercial PV modules with 25 years or more warranty lifetime on the field.[175] The current established operational lifetimes of PSCs of up to several months are not commercially viable yet.[176]

The instability issues of perovskites remain puzzles to be resolved upon further studies to elucidate the fundamentals in the material and device degradation mechanisms and the development of corresponding mitigation strategies. Although more research efforts are devoted to the perovskite stability study, the number of studies focusing on long-term outdoor stability tests of PSCs is still very limited. Thanks to the increasing global effort, the field of stability study has advanced significantly.[177-179] It is expected that the perovskite research community will come up with mitigation strategies to improve the reliability and durability of perovskite PV devices substantially.

4.5. Toxicity and Costs

A severe environmental concern of the halide perovskite materials for their future commercialization is their constituents that contain water soluble and toxic heavy metal compounds. Studies show that both Pb and Sn can cause detrimental environmental and human health issues,[180-182] raising significant concerns on wide deployment of the emerging PV technology. Even though the metal content in the perovskite PV modules is low, the leaching of heavy metals from perovskite devices can still cause highly undesirable environmental issues.[183, 184] Therefore, proper encapsulation techniques to lock Pb inside the module are needed to circumvent this problem.[95, 185] The compact TCO rear electrodes used in bifacial PSCs have their inherent advantages in preventing water ingress and leaching of metal content

in perovskites. Moreover, PV module recycling is not only a demand but a necessity at the end of the life cycle to minimize the negative environmental impacts.[186, 187]

In general, bifacial PSCs have slightly higher manufacture costs,[15] EPBT, and environmental impacts than their monofacial counterparts due to the use of two TCO electrodes.[107] However, bifacial configuration can enable up to 26% annual energy yield increase compared with monofacial devices.[107] The higher energy gain combined with enhanced device durability can eventually lead to better economic and environmental performance of bifacial perovskite PV modules than their monofacial counterparts. Because of these cost advantages, bifacial PSCs are still expected to outperform c-Si PV in the perspective of economic and environmental costs in the future.[107] Moreover, bifacial perovskite/Si tandem cells also show cost advantages to monofacial Si modules if long-term stability can be demonstrated.[115]

5. Outlook and Conclusion

Bifacial solar cells are the future of PV technologies and have been becoming the focus of many top-tier PV manufacturers in the market.[5] For the emerging perovskite PV technology, the time to consider moving to the bifacial cells and modules has come. The prospect of bifacial PSCs is promising because they hold the potential to deliver higher output powers for longer module lifetimes at the cost of a minimum increase in the manufacturing cost than their monofacial equivalents. The excellent optoelectronic properties of metal halide perovskites make them ideal candidates for fabricating high-efficiency and stable bifacial solar cells. High-power PV modules are essential to reduce solar electricity costs by minimizing the associated balance of system costs. Additionally, enhanced long-term stability is expected for bifacial PSCs owing to the self-encapsulation and chemical robustness of the TCO electrodes. Both benefits reduce the LCOE of PSCs, which will open a pathway for the commercialization of the perovskite PV.

Despite the promise, the potential benefits of bifacial perovskite PV can only be realized when many areas of development challenges and fundamental issues of materials, devices, and manufacturing are addressed. Hurdles to the widespread adoption of bifacial perovskite PVs include the various sources of optical and electrical power losses, lack of device reliability and durability, and the complexity and difficulty in bifacial module design and upscale production. The future of commercializing bifacial perovskite PV technology will depend on solving these challenges and issues. At present, the perovskite PV research community is working together to maintain the forward momentum of its research and development activities and hopes to address these issues via a close collaboration between academia and industry.[188] The efforts of the whole community help advance the field and accelerate the industrialization of PSCs. Finally, we predict that low-cost, high-efficiency bifacial perovskite PV modules will become one of the most cost-effective PV technology for electricity generation in the foreseeable future.

Acknowledgements

This material is based upon work supported by the U.S. Department of Energy's Office of Energy Efficiency and Renewable Energy (EERE) under the Solar Energy Technologies Office Award Numbers DE-EE0008753 and DE-EE0008790, and by the U.S. Air Force Research Laboratory under agreement number FA9453–19-C-1002. The U.S. Government is authorized to reproduce and distribute reprints for Governmental purposes notwithstanding any copyright notation thereon. Disclaimer: The views and conclusions contained herein are those of the authors and should not be interpreted as necessarily representing the official policies or endorsements, either expressed or implied, of the U.S. Air Force Research Laboratory or the U.S. Government.

Received: ((will be filled in by the editorial staff))
Revised: ((will be filled in by the editorial staff))
Published online: ((will be filled in by the editorial staff))

References

[1] IEA-PVPS, Snapshot of Global PV Markets, https://iea-pvps.org/snapshot-reports/snapshot-2021/, (Accessed on 21 August 2021).
[2] N. M. Haegel, H. Atwater, T. Barnes, C. Breyer, A. Burrell, Y.-M. Chiang, S. De Wolf, B. Dimmler, D. Feldman, S. Glunz, J. C. Goldschmidt, D. Hochschild, R. Inzunza, I. Kaizuka, B. Kroposki, S. Kurtz, S. Leu, R. Margolis, K. Matsubara, A. Metz, W. K. Metzger, M. Morjaria, S. Niki, S. Nowak, I. M. Peters, S. Philipps, T. Reindl, A. Richter, D. Rose, K. Sakurai, R. Schlatmann, M. Shikano, W. Sinke, R. Sinton, B. J. Stanbery, M. Topic, W. Tumas, Y. Ueda, J. van de Lagemaat, P. Verlinden, M. Vetter, E. Warren, M. Werner, M. Yamaguchi, A. W. Bett, *Science* **2019**, 364, 836.
[3] G. M. Wilson, M. Al-Jassim, W. K. Metzger, S. W. Glunz, P. Verlinden, G. Xiong, L. M. Mansfield, B. J. Stanbery, K. Zhu, Y. Yan, J. J. Berry, A. J. Ptak, F. Dimroth, B. M. Kayes, A. C. Tamboli, R. Peibst, K. Catchpole, M. O. Reese, C. S. Klinga, P. Denholm, M. Morjaria, M. G. Deceglie, J. M. Freeman, M. A. Mikofski, D. C. Jordan, G. TamizhMani, D. B. Sulas-Kern, *J. Phys. D: Appl. Phys.* **2020**, 53, 493001.
[4] T. S. Liang, M. Pravettoni, C. Deline, J. S. Stein, R. Kopecek, J. P. Singh, W. Luo, Y. Wang, A. G. Aberle, Y. S. Khoo, *Energy Environ. Sci.* **2019**, 12, 116.
[5] R. Kopecek, J. Libal, *Energies* **2021**, 14, 2076.
[6] NREL, Solar Cell Efficiency Chart, https://www.nrel.gov/pv/cell-efficiency.html, (Accessed on 6 July 2019).
[7] J. Y. Kim, J.-W. Lee, H. S. Jung, H. Shin, N.-G. Park, *Chem. Rev.* **2020**, 120, 7867.
[8] Z. Li, T. R. Klein, D. H. Kim, M. Yang, J. J. Berry, M. F. A. M. van Hest, K. Zhu, *Nat. Rev. Mater.* **2018**, 3, 18017.
[9] Z. Song, C. L. McElvany, A. B. Phillips, I. Celik, P. W. Krantz, S. C. Watthage, G. K. Liyanage, D. Apul, M. J. Heben, *Energy Environ. Sci.* **2017**, 10, 1297.
[10] I. Mathews, S. Sofia, E. Ma, J. Jean, H. S. Laine, S. C. Siah, T. Buonassisi, I. M. Peters, *Joule* **2020**, 4, 822.
[11] J. P. Singh, T. M. Walsh, A. G. Aberle, *Prog. Photovoltaics* **2014**, 22, 903.
[12] M. Rauer, A. Schmid, F. Guo, F. Neuberger, P. Gebhardt, J. Hohl-Ebinger, "Comprehensive Evaluation of IEC Measurement Procedures for Bifacial Solar Cells and Modules", presented at *Presented at the 37th European PV Solar Energy Conference and Exhibition*, 2020.
[13] H. Ohtsuka, M. Sakamoto, M. Koyama, K. Tsutsui, T. Uematsu, Y. Yazawa, *Prog. Photovoltaics* **2001**, 9, 1.
[14] M. Rauer, F. Guo, J. Hohl-Ebinger, "Accurate measurement of bifacial solar cells with single-and both-sided illumination", presented at *36th European PV Solar Energy Conference and Exhibition*, 2019.
[15] Z. Song, C. Chen, C. Li, S. Rijal, L. Chen, Y. Li, Y. Yan, *Sustainable Energy Fuels* **2021**, 5, 2865.
[16] Q. Lin, Z. Wang, H. J. Snaith, M. B. Johnston, L. M. Herz, *Adv. Sci.* **2018**, 5, 1700792.
[17] R. Guerrero-Lemus, R. Vega, T. Kim, A. Kimm, L. E. Shephard, *Renewable Sustainable Energy Rev.* **2016**, 60, 1533.
[18] M. Rauer, J. Greulich, N. Wöhrle, J. Hohl-Ebinger, H. Sträter, "Bifacial Solar Cells under Single-and Double-Sided Illumination: Effect of Non-Linearity in Short-Circuit Current", presented at *4th bifiPV workshop, Constance, Germany*, 2017.
[19] A. B. Phillips, K. K. Subedi, G. K. Liyanage, F. K. Alfadhili, R. J. Ellingson, M. J. Heben, *ACS Appl. Energy Mater.* **2020**, 3, 6072.
[20] K. K. Subedi, E. Bastola, I. Subedi, Z. Song, K. P. Bhandari, A. B. Phillips, N. J. Podraza, M. J. Heben, R. J. Ellingson, *Sol. Energy Mater. Sol. Cells* **2018**, 186, 227.

[21] K. K. Subedi, A. B. Phillips, N. Shrestha, F. K. Alfadhili, A. Osella, I. Subedi, R. A. Awni, E. Bastola, Z. Song, D.-B. Li, R. W. Collins, Y. Yan, N. J. Podraza, M. J. Heben, R. J. Ellingson, *Nano Energy* **2021**, 83, 105827.
[22] F. He, J. Li, S. Lin, W. Long, L. Wu, X. Hao, J. Zhang, L. Feng, *Solar Energy* **2021**, 214, 196.
[23] X. Wu, J. Zhou, A. Duda, J. C. Keane, T. A. Gessert, Y. Yan, R. Noufi, *Prog. Photovoltaics* **2006**, 14, 471.
[24] M. Mazzer, S. Rampino, G. Spaggiari, F. Annoni, D. Bersani, F. Bissoli, M. Bronzoni, M. Calicchio, E. Gombia, A. Kingma, F. Pattini, E. Gilioli, *Sol. Energy Mater. Sol. Cells* **2017**, 166, 247.
[25] J. Keller, W.-C. Chen, L. Riekehr, T. Kubart, T. Törndahl, M. Edoff, *Prog. Photovoltaics* **2018**, 26, 846.
[26] M. J. Shin, A. Lee, A. Cho, K. Kim, S. K. Ahn, J. H. Park, J. Yoo, J. H. Yun, J. Gwak, D. Shin, I. Jeong, J.-S. Cho, *Nano Energy* **2021**, 82, 105729.
[27] S.-Y. Chang, P. Cheng, G. Li, Y. Yang, *Joule* **2018**, 2, 1039.
[28] Z. Hu, J. Wang, X. Ma, J. Gao, C. Xu, K. Yang, Z. Wang, J. Zhang, F. Zhang, *Nano Energy* **2020**, 78, 105376.
[29] M. Godfroy, J. Liotier, V. M. Mwalukuku, D. Joly, Q. Huaulmé, L. Cabau, C. Aumaitre, Y. Kervella, S. Narbey, F. Oswald, E. Palomares, C. A. González Flores, G. Oskam, R. Demadrille, *Sustainable Energy Fuels* **2021**, 5, 144.
[30] Q. Huaulmé, V. M. Mwalukuku, D. Joly, J. Liotier, Y. Kervella, P. Maldivi, S. Narbey, F. Oswald, A. J. Riquelme, J. A. Anta, R. Demadrille, *Nat. Energy* **2020**, 5, 468.
[31] S. K. Meerdink, S. J. Hook, D. A. Roberts, E. A. Abbott, *Remote Sens. Environ.* **2019**, 230, 111196.
[32] T. C. R. Russell, R. Saive, A. Augusto, S. G. Bowden, H. A. Atwater, *IEEE J. Photovolt.* **2017**, 7, 1611.
[33] R. Kopecek, J. Libal, *Nat. Energy* **2018**, 3, 443.
[34] A. Cuevas, A. Luque, J. Eguren, J. del Alamo, *Solar Energy* **1982**, 29, 419.
[35] W.-J. Yin, J.-H. Yang, J. Kang, Y. Yan, S.-H. Wei, *J. Mater. Chem. A* **2015**, 3, 8926.
[36] Z. Xiao, Z. Song, Y. Yan, *Adv. Mater.* **2019**.
[37] W.-J. Yin, T. Shi, Y. Yan, *J. Phys. Chem. C* **2015**, 119, 5253.
[38] W.-J. Yin, T. Shi, Y. Yan, *Adv. Mater.* **2014**, 26, 4653.
[39] R. E. Brandt, J. R. Poindexter, P. Gorai, R. C. Kurchin, R. L. Z. Hoye, L. Nienhaus, M. W. B. Wilson, J. A. Polizzotti, R. Sereika, R. Žaltauskas, L. C. Lee, J. L. MacManus-Driscoll, M. Bawendi, V. Stevanović, T. Buonassisi, *Chem. Mater.* **2017**, 29, 4667.
[40] D. W. deQuilettes, K. Frohna, D. Emin, T. Kirchartz, V. Bulovic, D. S. Ginger, S. D. Stranks, *Chem. Rev.* **2019**, 119, 11007.
[41] W. Shockley, W. T. Read, *Phys. Rev.* **1952**, 87, 835.
[42] R. N. Hall, *Phys. Rev.* **1952**, 87, 387.
[43] W.-J. Yin, T. Shi, Y. Yan, *Appl. Phys. Lett.* **2014**, 104, 063903.
[44] M. Samiee, S. Konduri, B. Ganapathy, R. Kottokkaran, H. A. Abbas, A. Kitahara, P. Joshi, L. Zhang, M. Noack, V. Dalal, *Appl. Phys. Lett.* **2014**, 105, 153502.
[45] X. Yang, Y. Fu, R. Su, Y. Zheng, Y. Zhang, W. Yang, M. Yu, P. Chen, Y. Wang, J. Wu, D. Luo, Y. Tu, L. Zhao, Q. Gong, R. Zhu, *Adv. Mater.* **2020**, 32, 2002585.
[46] E. Gutierrez-Partida, H. Hempel, S. Caicedo-Dávila, M. Raoufi, F. Peña-Camargo, M. Grischek, R. Gunder, J. Diekmann, P. Caprioglio, K. O. Brinkmann, H. Köbler, S. Albrecht, T. Riedl, A. Abate, D. Abou-Ras, T. Unold, D. Neher, M. Stolterfoht, *ACS Energy Lett.* **2021**, 6, 1045.
[47] D. W. deQuilettes, S. Koch, S. Burke, R. K. Paranji, A. J. Shropshire, M. E. Ziffer, D. S. Ginger, *ACS Energy Lett.* **2016**, 1, 438.

[48] D. L. McGott, C. P. Muzzillo, C. L. Perkins, J. J. Berry, K. Zhu, J. N. Duenow, E. Colegrove, C. A. Wolden, M. O. Reese, *Joule* **2021**, 5, 1057.
[49] F. Brivio, K. T. Butler, A. Walsh, M. van Schilfgaarde, *Phys. Rev. B* **2014**, 89, 155204.
[50] G. Giorgi, J.-I. Fujisawa, H. Segawa, K. Yamashita, *J. Phys. Chem. Lett.* **2013**, 4, 4213.
[51] P. Umari, E. Mosconi, F. De Angelis, *Sci. Rep.* **2014**, 4, 4467.
[52] O. Gunawan, S. R. Pae, D. M. Bishop, Y. Virgus, J. H. Noh, N. J. Jeon, Y. S. Lee, X. Shao, T. Todorov, D. B. Mitzi, B. Shin, *Nature* **2019**, 575, 151.
[53] J. Euvrard, O. Gunawan, D. B. Mitzi, *Adv. Energy Mater.* **2019**.
[54] D. Shi, V. Adinolfi, R. Comin, M. Yuan, E. Alarousu, A. Buin, Y. Chen, S. Hoogland, A. Rothenberger, K. Katsiev, Y. Losovyj, X. Zhang, P. A. Dowben, O. F. Mohammed, E. H. Sargent, O. M. Bakr, *Science* **2015**, 347, 519.
[55] R. Su, Z. Xu, J. Wu, D. Luo, Q. Hu, W. Yang, X. Yang, R. Zhang, H. Yu, T. P. Russell, Q. Gong, W. Zhang, R. Zhu, *Nat. Commun.* **2021**, 12, 2479.
[56] L. M. Herz, *ACS Energy Lett.* **2017**, 2, 1539.
[57] S. D. Stranks, G. E. Eperon, G. Grancini, C. Menelaou, M. J. P. Alcocer, T. Leijtens, L. M. Herz, A. Petrozza, H. J. Snaith, *Science* **2013**, 342, 341.
[58] N. Shrestha, Z. Song, C. Chen, E. Bastola, X. Wang, Y. Yan, R. J. Ellingson, *J. Phys. Chem. Lett.* **2020**, 11, 121.
[59] M. S. Tumusange, B. Subedi, C. Chen, M. M. Junda, Z. Song, Y. Yan, N. J. Podraza, *Materials* **2021**, 14, 4054.
[60] Z. Song, S. C. Watthage, A. B. Phillips, M. J. Heben, *J. Photonics Energy* **2016**, 6, 022001.
[61] P. Lopez-Varo, J. A. Jiménez-Tejada, M. García-Rosell, S. Ravishankar, G. Garcia-Belmonte, J. Bisquert, O. Almora, *Adv. Energy Mater.* **2018**, 8, 1702772.
[62] F. Staub, H. Hempel, J.-C. Hebig, J. Mock, U. W. Paetzold, U. Rau, T. Unold, T. Kirchartz, *Phys. Rev. Appl.* **2016**, 6, 044017.
[63] E. Aydin, M. De Bastiani, S. De Wolf, *Adv. Mater.* **2019**, 31, 1900428.
[64] M. B. Johnston, L. M. Herz, *Acc. Chem. Res.* **2016**, 49, 146.
[65] Z. Ni, C. Bao, Y. Liu, Q. Jiang, W.-Q. Wu, S. Chen, X. Dai, B. Chen, B. Hartweg, Z. Yu, Z. Holman, J. Huang, *Science* **2020**, 367, 1352.
[66] L. K. Ono, S. Liu, Y. Qi, *Angew. Chem., Int. Ed.* **2020**, 59, 6676.
[67] D. Luo, R. Su, W. Zhang, Q. Gong, R. Zhu, *Nat. Rev. Mater.* **2020**, 5, 44.
[68] B. Hoex, S. B. S. Heil, E. Langereis, M. C. M. v. d. Sanden, W. M. M. Kessels, *Appl. Phys. Lett.* **2006**, 89, 042112.
[69] M. Burgelman, P. Nollet, S. Degrave, *Thin Solid Films* **2000**, 361–362, 527.
[70] F. Fu, T. Feurer, T. P. Weiss, S. Pisoni, E. Avancini, C. Andres, S. Buecheler, A. N. Tiwari, *Nat. Energy* **2016**, 2, 16190.
[71] M. Najafi, V. Zardetto, D. Zhang, D. Koushik, M. S. Dörenkämper, M. Creatore, R. Andriessen, P. Poodt, S. Veenstra, *Solar RRL* **2018**, 2, 1800147.
[72] H. Wang, H. A. Dewi, T. M. Koh, A. Bruno, S. Mhaisalkar, N. Mathews, *ACS Appl. Energy Mater.* **2020**, 12, 484.
[73] A. J. Bett, K. M. Winkler, M. Bivour, L. Cojocaru, Ö. Ş. Kabakli, P. S. C. Schulze, G. Siefer, L. Tutsch, M. Hermle, S. W. Glunz, J. C. Goldschmidt, *ACS Appl. Energy Mater.* **2019**, 11, 45796.
[74] M. Powalla, S. Paetel, E. Ahlswede, R. Wuerz, C. D. Wessendorf, T. M. Friedlmeier, *Appl. Phys. Rev.* **2018**, 5, 041602.
[75] R. Noufi, K. Zweibel, "High-Efficiency CdTe and CIGS Thin-Film Solar Cells: Highlights and Challenges", presented at *2006 IEEE 4th World Conference on Photovoltaic Energy Conference*, 7-12 May 2006, 2006.

[76] L. Kranz, C. Gretener, J. Perrenoud, R. Schmitt, F. Pianezzi, F. La Mattina, P. Blösch, E. Cheah, A. Chirilă, C. M. Fella, H. Hagendorfer, T. Jäger, S. Nishiwaki, A. R. Uhl, S. Buecheler, A. N. Tiwari, *Nat. Commun.* **2013**, 4, 2306.
[77] Y. Li, G. Yin, Y. Gao, T. Köhler, J. Lucaßen, M. Schmid, *Sol. Energy Mater. Sol. Cells* **2021**, 223, 110969.
[78] R. K. Kothandaraman, Y. Jiang, T. Feurer, A. N. Tiwari, F. Fu, *Small Methods* **2020**, 4, 2000395.
[79] J. A. Raiford, R. A. Belisle, K. A. Bush, R. Prasanna, A. F. Palmstrom, M. D. McGehee, S. F. Bent, *Sustainable Energy Fuels* **2019**, 3, 1517.
[80] F. Fu, T. Feurer, T. Jäger, E. Avancini, B. Bissig, S. Yoon, S. Buecheler, A. N. Tiwari, *Nat. Commun.* **2015**, 6, 8932.
[81] C. C. Boyd, R. Cheacharoen, K. A. Bush, R. Prasanna, T. Leijtens, M. D. McGehee, *ACS Energy Lett.* **2018**, 3, 1772.
[82] J. Huang, S. Tan, P. D. Lund, H. Zhou, *Energy Environ. Sci.* **2017**, 10, 2284.
[83] Z. Song, N. Shrestha, S. C. Watthage, G. K. Liyanage, Z. S. Almutawah, R. H. Ahangharnejhad, A. B. Phillips, R. J. Ellingson, M. J. Heben, *J. Phys. Chem. Lett.* **2018**, 9, 6312.
[84] R. Hosseinian Ahangharnejhad, Z. Song, T. Mariam, J. J. Gardner, G. K. Liyanage, Z. S. Almutawah, B. M. M. Anwar, M. Junda, N. J. Podraza, A. B. Phillips, Y. Yan, M. J. Heben, *ACS Appl. Energy Mater.* **2021**, 4, 7571.
[85] E. J. Juarez-Perez, L. K. Ono, M. Maeda, Y. Jiang, Z. Hawash, Y. Qi, *J. Mater. Chem. A* **2018**, 6, 9604.
[86] Z. Song, C. Wang, A. B. Phillips, C. R. Grice, D. Zhao, Y. Yu, C. Chen, C. Li, X. Yin, R. Ellingson, M. Heben, Y. Yan, *Sustainable Energy Fuels* **2018**, 2, 2460.
[87] W. Ming, D. Yang, T. Li, L. Zhang, M.-H. Du, *Adv. Sci.* **2018**, 5, 1700662.
[88] H. Back, G. Kim, J. Kim, J. Kong, T. K. Kim, H. Kang, H. Kim, J. Lee, S. Lee, K. Lee, *Energy Environ. Sci.* **2016**, 9, 1258.
[89] L. Zhao, R. A. Kerner, Z. Xiao, Y. L. Lin, K. M. Lee, J. Schwartz, B. P. Rand, *ACS Energy Lett.* **2016**, 1, 595.
[90] K. A. Bush, C. D. Bailie, Y. Chen, A. R. Bowring, W. Wang, W. Ma, T. Leijtens, F. Moghadam, M. D. McGehee, *Adv. Mater.* **2016**, 28, 3937.
[91] C. C. Boyd, R. Cheacharoen, T. Leijtens, M. D. McGehee, *Chem. Rev.* **2019**, 119, 3418.
[92] K. Brinkmann, J. Zhao, N. Pourdavoud, T. Becker, T. Hu, S. Olthof, K. Meerholz, L. Hoffmann, T. Gahlmann, R. Heiderhoff, *Nat. Commun.* **2017**, 8, 1.
[93] I. S. Kim, D. H. Cao, D. B. Buchholz, J. D. Emery, O. K. Farha, J. T. Hupp, M. G. Kanatzidis, A. B. F. Martinson, *Nano Lett.* **2016**, 16, 7786.
[94] Y. Cheng, X. Liu, Z. Guan, M. Li, Z. Zeng, H.-W. Li, S.-W. Tsang, A. G. Aberle, F. Lin, *Adv. Mater.* **2021**, 33, 2006170.
[95] Y. Jiang, L. Qiu, E. J. Juarez-Perez, L. K. Ono, Z. Hu, Z. Liu, Z. Wu, L. Meng, Q. Wang, Y. Qi, *Nat. Energy* **2019**, 4, 585.
[96] R. Cheacharoen, N. Rolston, D. Harwood, K. A. Bush, R. H. Dauskardt, M. D. McGehee, *Energy Environ. Sci.* **2018**, 11, 144.
[97] R. Cheacharoen, C. C. Boyd, G. F. Burkhard, T. Leijtens, J. A. Raiford, K. A. Bush, S. F. Bent, M. D. McGehee, *Sustainable Energy Fuels* **2018**, 2, 2398.
[98] R. Prasanna, T. Leijtens, S. P. Dunfield, J. A. Raiford, E. J. Wolf, S. A. Swifter, J. Werner, G. E. Eperon, C. de Paula, A. F. Palmstrom, C. C. Boyd, M. F. A. M. van Hest, S. F. Bent, G. Teeter, J. J. Berry, M. D. McGehee, *Nat. Energy* **2019**, 4, 939.
[99] E. Bi, Z. Song, C. Li, Z. Wu, Y. Yan, *Trends Chem.* **2021**, 3, 575.

[100] C. Besleaga, L. E. Abramiuc, V. Stancu, A. G. Tomulescu, M. Sima, L. Trinca, N. Plugaru, L. Pintilie, G. A. Nemnes, M. Iliescu, H. G. Svavarsson, A. Manolescu, I. Pintilie, *J. Phys. Chem. Lett.* **2016**, 7, 5168.
[101] J. Li, Q. Dong, N. Li, L. Wang, *Adv. Energy Mater.* **2017**, 7, 1602922.
[102] Y. Kato, L. K. Ono, M. V. Lee, S. Wang, S. R. Raga, Y. Qi, *Adv. Mater. Interfaces* **2015**, 2, 1500195.
[103] K. Domanski, J.-P. Correa-Baena, N. Mine, M. K. Nazeeruddin, A. Abate, M. Saliba, W. Tress, A. Hagfeldt, M. Grätzel, *ACS Nano* **2016**, 10, 6306.
[104] S. Wu, R. Chen, S. Zhang, B. H. Babu, Y. Yue, H. Zhu, Z. Yang, C. Chen, W. Chen, Y. Huang, S. Fang, T. Liu, L. Han, W. Chen, *Nat. Commun.* **2019**, 10, 1161.
[105] N. N. Udalova, E. M. Nemygina, E. A. Zharenova, A. S. Tutantsev, A. A. Sudakov, A. Y. Grishko, N. A. Belich, E. A. Goodilin, A. B. Tarasov, *J. Phys. Chem. C* **2020**, 124, 24601.
[106] M. Cai, Y. Wu, H. Chen, X. Yang, Y. Qiang, L. Han, *Adv. Sci.* **2017**, 4, 1600269.
[107] R. Hosseinian Ahangharnejhad, W. Becker, J. Jones, A. Anctil, Z. Song, A. Phillips, M. J. Heben, I. Celik, *Cell Rep. Phys. Sci.* **2020**, 1, 100216.
[108] C. Deline, S. MacAlpine, B. Marion, F. Toor, A. Asgharzadeh, J. S. Stein, *IEEE J. Photovolt.* **2017**, 7, 575.
[109] C. A. Deline, S. Ayala Pelaez, W. F. Marion, W. R. Sekulic, M. A. Woodhouse, J. Stein, Bifacial PV system performance: separating fact from fiction, https://www.nrel.gov/docs/fy19osti/74090.pdf, (Accessed on 21 August 2021).
[110] S. Rahmany, L. Etgar, *ACS Energy Lett.* **2020**, 5, 1519.
[111] D. Liu, C. Yang, R. R. Lunt, *Joule* **2018**, 2, 1827.
[112] H. Wang, J. Li, H. A. Dewi, N. Mathews, S. Mhaisalkar, A. Bruno, *J. Phys. Chem. Lett.* **2021**, 12, 1321.
[113] C. Hanmandlu, C.-Y. Chen, K. M. Boopathi, H.-W. Lin, C.-S. Lai, C.-W. Chu, *ACS Appl. Energy Mater.* **2017**, 9, 32635.
[114] M. Mujahid, C. Chen, J. Zhang, C. Li, Y. Duan, *InfoMat* **2021**, 3, 101.
[115] G. Coletti, S. L. Luxembourg, L. J. Geerligs, V. Rosca, A. R. Burgers, Y. Wu, L. Okel, M. Kloos, F. J. K. Danzl, M. Najafi, D. Zhang, I. Dogan, V. Zardetto, F. Di Giacomo, J. Kroon, T. Aernouts, J. Hüpkes, C. H. Burgess, M. Creatore, R. Andriessen, S. Veenstra, *ACS Energy Lett.* **2020**, 5, 1676.
[116] R. Wang, T. Huang, J. Xue, J. Tong, K. Zhu, Y. Yang, *Nat. Photonics* **2021**, 15, 411.
[117] Z. Song, C. Chen, C. Li, R. A. Awni, D. Zhao, Y. Yan, *Semicond. Sci. Technol.* **2019**, 34, 093001.
[118] M. Jošt, L. Kegelmann, L. Korte, S. Albrecht, *Adv. Energy Mater.* **2020**, 10, 1904102.
[119] K. M. Yeom, S. U. Kim, M. Y. Woo, J. H. Noh, S. H. Im, *Adv. Mater.* **2020**, 32, 2002228.
[120] S. Kim, T. T. Trinh, J. Park, D. P. Pham, S. Lee, H. B. Do, N. N. Dang, V.-A. Dao, J. Kim, J. Yi, *Sci. Rep.* **2021**, 11, 15524.
[121] R. Asadpour, R. V. K. Chavali, M. Ryyan Khan, M. A. Alam, *Appl. Phys. Lett.* **2015**, 106, 243902.
[122] M. De Bastiani, A. J. Mirabelli, Y. Hou, F. Gota, E. Aydin, T. G. Allen, J. Troughton, A. S. Subbiah, F. H. Isikgor, J. Liu, L. Xu, B. Chen, E. Van Kerschaver, D. Baran, B. Fraboni, M. F. Salvador, U. W. Paetzold, E. H. Sargent, S. De Wolf, *Nat. Energy* **2021**, 6, 167.
[123] K. Jäger, P. Tillmann, E. A. Katz, C. Becker, *Solar RRL* **2021**, 5, 2000628.
[124] J.-D. Chen, T.-Y. Jin, Y.-Q. Li, J.-X. Tang, *Nanoscale* **2019**, 11, 18517.
[125] M.-c. Kim, S. Jang, J. Choi, S. M. Kang, M. Choi, *Nano-Micro Lett.* **2019**, 11, 53.
[126] S. Manzoor, Z. J. Yu, A. Ali, W. Ali, K. A. Bush, A. F. Palmstrom, S. F. Bent, M. D. McGehee, Z. C. Holman, *Sol. Energy Mater. Sol. Cells* **2017**, 173, 59.
[127] M. Jošt, S. Albrecht, L. Kegelmann, C. M. Wolff, F. Lang, B. Lipovšek, J. Krč, L. Korte, D. Neher, B. Rech, M. Topič, *ACS Photonics* **2017**, 4, 1232.

[128] B. B. V. Aken, M. J. Jansen, N. J. J. Dekker, "Reliability and energy output of bifacial modules", presented at *2013 IEEE 39th Photovoltaic Specialists Conference (PVSC)*, 16-21 June 2013, 2013.
[129] K. Deng, Z. Liu, M. Wang, L. Li, *Adv. Funct. Mater.* **2019**, 29, 1900830.
[130] R. Siavash Moakhar, S. Gholipour, S. Masudy-Panah, A. Seza, A. Mehdikhani, N. Riahi-Noori, S. Tafazoli, N. Timasi, Y.-F. Lim, M. Saliba, *Adv. Sci.* **2020**, 7, 1902448.
[131] Y. Deng, Q. Wang, Y. Yuan, J. Huang, *Mater. Horiz.* **2015**, 2, 578.
[132] K.-T. Lee, M. Fukuda, S. Joglekar, L. J. Guo, *J. Mater. Chem. C* **2015**, 3, 5377.
[133] Y. Jiang, T. Feurer, R. Carron, G. T. Sevilla, T. Moser, S. Pisoni, R. Erni, M. D. Rossell, M. Ochoa, R. Hertwig, A. N. Tiwari, F. Fu, *ACS Nano* **2020**, 14, 7502.
[134] Z. Ying, X. Yang, J. Zheng, Y. Zhu, J. Xiu, W. Chen, C. Shou, J. Sheng, Y. Zeng, B. Yan, H. Pan, J. Ye, Z. He, *J. Mater. Chem. A* **2021**, 9, 12009.
[135] S.-H. Lim, H.-J. Seok, M.-J. Kwak, D.-H. Choi, S.-K. Kim, D.-H. Kim, H.-K. Kim, *Nano Energy* **2021**, 82, 105703.
[136] F. Liang, Z. Ying, Y. Lin, B. Tu, Z. Zhang, Y. Zhu, H. Pan, H. Li, L. Luo, O. Ageev, Z. He, *Adv. Mater. Interfaces* **2020**, 7, 2000591.
[137] D. Chen, S. Pang, L. Zhou, X. Li, A. Su, W. Zhu, J. Chang, J. Zhang, C. Zhang, Y. Hao, *J. Mater. Chem. A* **2019**, 7, 15156.
[138] Y.-J. Chen, M.-H. Li, J.-C.-A. Huang, P. Chen, *J. Mater. Chem. C* **2018**, 6, 6280.
[139] C. O. Ramírez Quiroz, I. Levchuk, C. Bronnbauer, M. Salvador, K. Forberich, T. Heumüller, Y. Hou, P. Schweizer, E. Spiecker, C. J. Brabec, *J. Mater. Chem. A* **2015**, 3, 24071.
[140] C.-Y. Chang, K.-T. Lee, W.-K. Huang, H.-Y. Siao, Y.-C. Chang, *Chem. Mater.* **2015**, 27, 5122.
[141] Z. Liu, P. You, C. Xie, G. Tang, F. Yan, *Nano Energy* **2016**, 28, 151.
[142] P. You, Z. Liu, Q. Tai, S. Liu, F. Yan, *Adv. Mater.* **2015**, 27, 3632.
[143] F. R. Li, Y. Xu, W. Chen, S. H. Xie, J. Y. Li, *J. Mater. Chem. A* **2017**, 5, 10374.
[144] B. Subedi, Z. Song, C. Chen, C. Li, K. Ghimire, M. M. Junda, I. Subedi, Y. Yan, N. J. Podraza, *ACS Appl. Energy Mater.* **2021**, 13, 4923.
[145] H. Fujiwara, M. Kato, M. Tamakoshi, T. Miyadera, M. Chikamatsu, *Phys. Status Solidi A* **2018**, 215, 1700730.
[146] E. Della Gaspera, Y. Peng, Q. C. Hou, L. Spiccia, U. Bach, J. J. Jasieniak, Y. B. Cheng, in *Nano Energy*, Vol. 13, 2015, 249.
[147] T. Wahl, J. Hanisch, S. Meier, M. Schultes, E. Ahlswede, *Org. Electron.* **2018**, 54, 48.
[148] R. A. Jagt, T. N. Huq, S. A. Hill, M. Thway, T. Liu, M. Napari, B. Roose, K. Gałkowski, W. Li, S. F. Lin, S. D. Stranks, J. L. MacManus-Driscoll, R. L. Z. Hoye, *ACS Energy Lett.* **2020**, 5, 2456.
[149] H. Eggers, F. Schackmar, T. Abzieher, Q. Sun, U. Lemmer, Y. Vaynzof, B. S. Richards, G. Hernandez-Sosa, U. W. Paetzold, *Adv. Energy Mater.* **2020**, 10, 1903184.
[150] Z. Liu, L. Qiu, E. J. Juarez-Perez, Z. Hawash, T. Kim, Y. Jiang, Z. Wu, S. R. Raga, L. K. Ono, S. Liu, Y. Qi, *Nat. Commun.* **2018**, 9, 3880.
[151] C. M. Wolff, P. Caprioglio, M. Stolterfoht, D. Neher, *Adv. Mater.* **2019**, 31, 1902762.
[152] D. Głowienka, D. Zhang, F. Di Giacomo, M. Najafi, S. Veenstra, J. Szmytkowski, Y. Galagan, *Nano Energy* **2020**, 67, 104186.
[153] A. Nakane, H. Tampo, M. Tamakoshi, S. Fujimoto, K. M. Kim, S. Kim, H. Shibata, S. Niki, H. Fujiwara, *J. Appl. Phys.* **2016**, 120, 064505.
[154] J. Werner, C. C. Boyd, T. Moot, E. J. Wolf, R. M. France, S. A. Johnson, M. F. A. M. van Hest, J. M. Luther, K. Zhu, J. J. Berry, M. D. McGehee, *Energy Environ. Sci.* **2020**, 13, 3393.
[155] M. Zhang, B. Wilkinson, Y. Liao, J. Zheng, C. F. J. Lau, J. Kim, J. Bing, M. A. Green, S. Huang, A. W.-Y. Ho-Baillie, *Joule* **2018**, 2, 2694.

[156] J. Werner, G. Dubuis, A. Walter, P. Löper, S.-J. Moon, S. Nicolay, M. Morales-Masis, S. De Wolf, B. Niesen, C. Ballif, *Sol. Energy Mater. Sol. Cells* **2015**, 141, 407.
[157] D. Zhao, C. Wang, Z. Song, Y. Yu, C. Chen, X. Zhao, K. Zhu, Y. Yan, *ACS Energy Lett.* **2018**, 3, 305.
[158] S. Albrecht, M. Saliba, J. P. Correa Baena, F. Lang, L. Kegelmann, M. Mews, L. Steier, A. Abate, J. Rappich, L. Korte, R. Schlatmann, M. K. Nazeeruddin, A. Hagfeldt, M. Gratzel, B. Rech, *Energy Environ. Sci.* **2016**, 9, 81.
[159] J. Zheng, C. F. J. Lau, H. Mehrvarz, F.-J. Ma, Y. Jiang, X. Deng, A. Soeriyadi, J. Kim, M. Zhang, L. Hu, X. Cui, D. S. Lee, J. Bing, Y. Cho, C. Chen, M. A. Green, S. Huang, A. W. Y. Ho-Baillie, *Energy Environ. Sci.* **2018**, 11, 2432.
[160] Y.-J. Noh, J.-G. Kim, S.-S. Kim, H.-K. Kim, S.-I. Na, *J. Power Sources* **2019**, 437, 226894.
[161] G. E. Eperon, T. Leijtens, K. A. Bush, R. Prasanna, T. Green, J. T.-W. Wang, D. P. McMeekin, G. Volonakis, R. L. Milot, R. May, A. Palmstrom, D. J. Slotcavage, R. A. Belisle, J. B. Patel, E. S. Parrott, R. J. Sutton, W. Ma, F. Moghadam, B. Conings, A. Babayigit, H.-G. Boyen, S. Bent, F. Giustino, L. M. Herz, M. B. Johnston, M. D. McGehee, H. J. Snaith, *Science* **2016**, 354, 861.
[162] Z. Ying, Y. Zhu, X. Feng, J. Xiu, R. Zhang, X. Ma, Y. Deng, H. Pan, Z. He, *Adv. Mater. Interfaces* **2021**, 8, 2001604.
[163] M. Jaysankar, W. Qiu, M. van Eerden, T. Aernouts, R. Gehlhaar, M. Debucquoy, U. W. Paetzold, J. Poortmans, *Adv. Energy Mater.* **2017**, 7, 1602807.
[164] S.-W. Lee, S. Bae, D. Kim, H.-S. Lee, *Adv. Mater.* **2020**, 32, 2002202.
[165] A. S. Subbiah, F. H. Isikgor, C. T. Howells, M. De Bastiani, J. Liu, E. Aydin, F. Furlan, T. G. Allen, F. Xu, S. Zhumagali, S. Hoogland, E. H. Sargent, I. McCulloch, S. De Wolf, *ACS Energy Lett.* **2020**, 5, 3034.
[166] Z. Yang, W. Zhang, S. Wu, H. Zhu, Z. Liu, Z. Liu, Z. Jiang, R. Chen, J. Zhou, Q. Lu, Z. Xiao, L. Shi, H. Chen, L. K. Ono, S. Zhang, Y. Zhang, Y. Qi, L. Han, W. Chen, *Sci. Adv.* **2021**, 7, eabg3749.
[167] J. Li, J. Dagar, O. Shargaieva, M. A. Flatken, H. Köbler, M. Fenske, C. Schultz, B. Stegemann, J. Just, D. M. Többens, A. Abate, R. Munir, E. Unger, *Adv. Energy Mater.* **2021**, 11, 2003460.
[168] S. Chen, X. Xiao, H. Gu, J. Huang, *Sci. Adv.* **2021**, 7, eabe8130.
[169] J. W. Yoo, J. Jang, U. Kim, Y. Lee, S.-G. Ji, E. Noh, S. Hong, M. Choi, S. I. Seok, *Joule* **2021**, 5, 2420.
[170] J. Zhang, T. Bu, J. Li, H. Li, Y. Mo, Z. Wu, Y. Liu, X.-L. Zhang, Y.-B. Cheng, F. Huang, *J. Mater. Chem. A* **2020**, 8, 8447.
[171] Y. Deng, X. Zheng, Y. Bai, Q. Wang, J. Zhao, J. Huang, *Nat. Energy* **2018**, 3, 560.
[172] Y. Y. Kim, T.-Y. Yang, R. Suhonen, A. Kemppainen, K. Hwang, N. J. Jeon, J. Seo, *Nat. Commun.* **2020**, 11, 5146.
[173] B. Dou, J. B. Whitaker, K. Bruening, D. T. Moore, L. M. Wheeler, J. Ryter, N. J. Breslin, J. J. Berry, S. M. Garner, F. S. Barnes, S. E. Shaheen, C. J. Tassone, K. Zhu, M. F. A. M. van Hest, *ACS Energy Lett.* **2018**, 3, 2558.
[174] J. F. Benitez-Rodriguez, D. Chen, M. Gao, R. A. Caruso, *Solar RRL* **2021**, 5, 2100341.
[175] M. A. Green, *Nat. Energy* **2016**, 1, 15015.
[176] M. V. Khenkin, E. A. Katz, A. Abate, G. Bardizza, J. J. Berry, C. Brabec, F. Brunetti, V. Bulović, Q. Burlingame, A. Di Carlo, R. Cheacharoen, Y.-B. Cheng, A. Colsmann, S. Cros, K. Domanski, M. Dusza, C. J. Fell, S. R. Forrest, Y. Galagan, D. Di Girolamo, M. Grätzel, A. Hagfeldt, E. von Hauff, H. Hoppe, J. Kettle, H. Köbler, M. S. Leite, S. Liu, Y.-L. Loo, J. M. Luther, C.-Q. Ma, M. Madsen, M. Manceau, M. Matheron, M. McGehee, R. Meitzner, M. K. Nazeeruddin, A. F. Nogueira, Ç. Odabaşı, A. Osherov, N.-G. Park, M. O. Reese, F. De Rossi, M. Saliba, U. S. Schubert, H. J. Snaith, S. D. Stranks, W. Tress, P. A.

Troshin, V. Turkovic, S. Veenstra, I. Visoly-Fisher, A. Walsh, T. Watson, H. Xie, R. Yıldırım, S. M. Zakeeruddin, K. Zhu, M. Lira-Cantu, *Nat. Energy* **2020**, 5, 35.
[177] M. Jošt, B. Lipovšek, B. Glažar, A. Al-Ashouri, K. Brecl, G. Matič, A. Magomedov, V. Getautis, M. Topič, S. Albrecht, *Adv. Energy Mater.* **2020**, 10, 2000454.
[178] E. Velilla, F. Jaramillo, I. Mora-Seró, *Nat. Energy* **2021**, 6, 54.
[179] E. Aydin, T. G. Allen, M. De Bastiani, L. Xu, J. Ávila, M. Salvador, E. Van Kerschaver, S. De Wolf, *Nat. Energy* **2020**, 5, 851.
[180] A. Babayigit, D. Duy Thanh, A. Ethirajan, J. Manca, M. Muller, H.-G. Boyen, B. Conings, *Sci. Rep.* **2016**, 6, 18721.
[181] A. Babayigit, A. Ethirajan, M. Muller, B. Conings, *Nat. Mater.* **2016**, 15, 247.
[182] L. Serrano-Lujan, N. Espinosa, T. T. Larsen-Olsen, J. Abad, A. Urbina, F. C. Krebs, *Adv. Energy Mater.* **2015**, 5, n/a.
[183] I. Celik, Z. Song, M. J. Heben, D. Apul, *J. Cleaner Prod.* **2017**, 186, 632.
[184] B. Hailegnaw, S. Kirmayer, E. Edri, G. Hodes, D. Cahen, *J. Phys. Chem. Lett.* **2015**, 6, 1543.
[185] X. Li, F. Zhang, H. He, J. J. Berry, K. Zhu, T. Xu, *Nature* **2020**, 578, 555.
[186] K. P. Goetz, A. D. Taylor, Y. J. Hofstetter, Y. Vaynzof, *ACS Appl. Energy Mater.* **2021**, 13, 1.
[187] X. Tian, S. D. Stranks, F. You, *Nature Sustainability* **2021**, 4, 821.
[188] NREL, News Release: NREL Helps Found Consortium to Boost Solar Perovskite Commercialization, https://www.nrel.gov/news/press/2020/nrel-helps-found-consortium-to-boost-solar-perovskite-commercialization.html, (Accessed on 21 August 2021).

Zhaoning Song is a Research Assistant Professor at the Wright Center for Photovoltaics Innovation and Commercialization (PVIC), The University of Toledo. He received his Ph. D. degree in Physics from The University of Toledo in 2016 and continued his research there. His current research work focuses on perovskite solar cells, photodetectors, and photoelectrochemical devices. His research interest includes device physics, device modeling, nanomaterial synthesis, thin-film semiconductors, and optoelectronics.

Yanfa Yan has been an Ohio Research Scholar Chair and Distinguish Professor in the Department of Physics and Astronomy at The University of Toledo, since 2011. Previously, he was a Principal Scientist at the National Renewable Energy Laboratory. He earned his Ph. D. in Physics from Wuhan University in 1993. His expertise includes thin-film solar cell fabrication, defect physics of semiconductors, and nanoscale characterization of microstructures, interfaces, and defects in thin-film photovoltaic materials. He is a Fellow of the American Physical Society.

The table of contents:

Metal halide perovskites are an ideal candidate for fabricating bifacial thin-film solar cells because of their outstanding optoelectronic properties and unique features of device physics. Bifacial perovskite solar cells hold the potential to simultaneously achieve higher energy yield and longer device stability than their monofacial equivalent, which provides a commercialization path for perovskite photovoltaics in the future.